Design, analysis, simulation and experimentation of a flexible spine quadruped

A THESIS

SUBMITTED FOR THE DEGREE OF

Master of Science (Engineering)

IN THE FACULTY OF ENGINEERING

by

Shounak Bhattacharya

Mechanical Engineering

Indian Institute of Science

BANGALORE – 560 012

December 31, 2017

©Shounak Bhattacharya

December 31, 2017

All rights reserved

TO

Robotics lab.

and

Dhrubo

CERTIFICATE

I hereby certify that the content embodied in this thesis titled **Design, analysis, simulation and experimentation of a flexible spine quadruped** has been carried out by Mr. Shounak Bhattacharya at the Indian Institute of Science, Bangalore under my supervision and that it has not been submitted elsewhere for the award of any degree or diploma.

Signature of the Thesis Supervisor: .....

Professor Ashitava Ghosal
Dept. of Mechanical Engineering
Indian Institute of Science, Bangalore

DECLARATION

I hereby declare that the content embodied in this thesis titled **Design, analysis, simulation and experimentation of a flexible spine quadruped** is the research carried out by me at the Department of Mechanical Engineering, Indian Institute of Science, Bangalore under the supervision Prof. Ashitava Ghosal, Department of Mechanical Engineering, IISc. In keeping with the general practice in reporting scientific observations, due acknowledgment has been made wherever the work described is based on the findings of other investigations.

Signature of the Author: .....

Shounak Bhattacharya
Robotics Lab.
Dept. of Mechanical Engineering
Indian Institute of Science, Bangalore

Acknowledgements

I take this opportunity to thank my advisor Prof. Ashitava Ghosal who has motivated and encouraged me all through the course of this thesis work. I appreciate his patience in explaining things to me especially when I made mistakes. I have learned many things from him, and without his valuable guidance, I would not have come this far. I would also like to thank the Department of Mechanical Engineering, Indian Institute of Science for all the facilities given to me and made my stay in the campus pleasant and fruitful. Sincere thanks goes to all the professors and staff members in IISc. For motivating, guiding and helping me during my stay in IISc. A special thanks goes to all my lab-mates especially to Arkadeep, Ashith S. Babu, Ashwin K.P., Mohit Acharya, Puneet Singh, Ravi Teja Chanamolu, Mithun S.Menon. Also, a special thanks goes to neighbor Ananda Sankar Chakrabarty who is a significant part of my life here in IISc. I also extend my gratitude to Robert Bosch center for cyber physical system(RBCCPS) for funding my project. Finally, I extend my appreciation to my parents, Saibal Bhattacharya and Ratna Bhattacharya, and family here Montada, Sudarsana boudi and Dhrub, and all other family members who have always been there by my side as pillars of support. I would also like to mention the members of "Khadok" group, without whom the experience of this institute would have been unfulfilled.
And finally, I would like to extend special gratitude to my roommate who kept my spirit up, (along with my neighbor's) even in the earliest hours of the morning.

Shounak Bhattacharya
Robotics Lab.
Department of Mechanical Engineering
Indian Institute of Science
Bangalore.

Abstract

Quadrupeds robots can move on uneven and rough terrain where mobile robots cannot venture. Although bipeds have more capabilities, they are inherently unstable and difficult to control. Most quadrupeds today are built with a rigid spine. In nature, however, all quadruped have a flexible spine, and it provides better agility and more efficiency in motion. This thesis deals with the study of the development of a method to develop a flexible spine for Quadruped robots. At first, we explore the idea of discretizing a continuous beam into multiple rigid and flexible body element. The flexible elements are considered to be linear torsional spring on a rotary joint (R). We developed a simple algebraic formulation to discretize a continuous beam in any desired number of rigid and flexible elements.We show that, for small deflection, this method covers all types of boundary condition generated in a beam formulation. Next, we exploit the idea of transforming the continuous structure into a rigid-flexible structure to generate spine-like structure for quadruped robot. We use ideas from structural optimization to produce a shape of the articulated structure that can support the desired load while providing the needed flexibility. The objective function used in the optimization represents the rigidity of the structure, and the constraints contained the flexibility desired. A gradient-based optimization method is used to obtain various structures under similar constraints for different endpoint flexibility. Additionally, we analyze the response time of the structure. It is shown that the desired response time can be obtained by introducing damping in various parts of the structure. Again a gradient-based optimization is used to obtain the damping in the structure to achieve the desired response time.

In the second part, we deal with the development of quadruped robots with the rigid and flexible spine. The CAD models of the robots created and simulated in the physics engine. Once validated, the segments and modules of the robots are manufactured and assembled with the servo motors. The controllers and power source are added afterward completing the design. The robots are both controlled with coupled nonlinear oscillator without any feedback. By controlling the coupling, we generated various gaits in the robots such as trot, bound and canter. In the simulation result, we found the velocity of the flexible spine quadruped is higher than a rigid spine quadruped for a bounding gait. In this part, we also describe the use of the optimal spine in the development of the quadruped and problems experienced while executing it in real life.

Contents

List of Tables

List of Figures

Chapter 1

Introduction

1.1 Motivation

The analysis, design and fabrication of quadruped robots are one of the key topics of interest in the field of robotics. This is motivated by four-legged animals which can carry large loads on their back and also navigate through rough terrains which are inaccessible to wheeled mobile robots. Several such legged robots have been designed and built (for example, HyQ2Max [1], ANYmal [2], Big-dog [3]). They mimic the motion of quadruped animals. Most of these robots have a rigid central structure along its primary axis, which reduces the flexibility of their body. The lack of flexibility reduces maneuverability and stride length. Motivated by nature, recently researchers have attempted to design an articulated spine for a quadruped robot[4] and this has shown encouraging results, in terms of energy efficiency and average running speed (see, for example, the MIT Cheetah [5],Lynx [6], Bobcat [7]). These designs can be classified into two broad categories, namely, active actuated spine [8] and passive flexible spine [9, 10]. In recent work, researchers [11] have also studied a bionic flexible body for side-wise bending.

(a) CheetahCub

(b) MIT Cheetah 2

(c) HyQ

Figure 1.1: Various rigid spine quadruped robots built so far

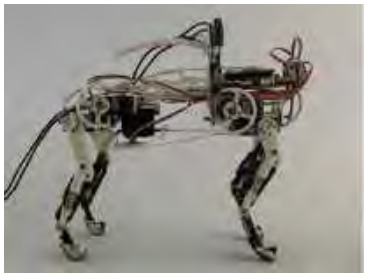

(a) Lynx SV3

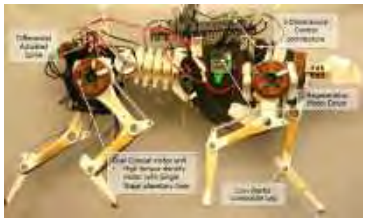

(b) MIT Cheetah

(c) Cheetah

Figure 1.2: Various flexible spine quadrupeds

1.2 Challenges in designing a flexible spine quadruped

The analysis and fabrication quadruped robots has drawn large amount of world wide interest with various groups working on the topic. Creating a flexible spine quadruped is very challenging, and so far, there has not been any formal way to design a flexible spine quadruped. Work done on MIT Cheetah and EPFL Lynx is one of the prominent example of flexible spine quadruped. Both however suffers from the issue of stability. The problem with stability arises due to two major reasons. First, The internal load experienced by the body is significant enough to cause deformation in the spine if it is no rigid enough. This results in undesired movement of spine even in gaits which does not require spine movement at all. Hence, the body becomes unstable. Also, the loading experienced by the body is much more than the static loading value of the structure. The second reason of instability is due to presence of undesired degrees of freedom in the spine, such as off plane bending and torsion. As there are no actuators in the direction of the undesired movement, there are no mechanism to correct the error generated due to these motions. In this work, we address the first issue with help of parameter optimization process and while designing the experimental model we experience the second issue.

1.3 Parameter optimization

In the field of designing structures by objective function minimization[12], parameter optimization is a standard procedure. Work done by Xu and Ananthasuresh[13], Zhou and Ting[14] have solved a similar problem but with a continuous beam. In these works, first, the variable was parameterized. Next, the desired objective was considered as a constraint in the optimization. Finally, an objective function was selected to be minimized. In reference [13], the ratio of *mutual strain energy* and *strain energy* is selected to be the objective function. Once the optimization problem is designed, gradient-based methods are used to determine the solution. In reference, [13] the parameters of a bezier curve and in [14] parameters of a wide curve were determined with the gradient-based approach. Finally, the

optimal solutions of these problems were used to design compliant mechanisms. The hardware model developed by the optimal solution shows desired properties provided as constraints earlier.

In this work, we pose the problem of rigidity and flexibility of the spine similarly. The desired objective, flexibility, is set as a constraint for the optimization problem and the rigidity, strain energy, is posed as the objective function. The solution of this problem provides the shape and nodal stiffness of the spine. Unlike the works in reference [13], this works deals with the multi-body system rather than a continuous beam.

1.4 Contribution of this thesis

The goal of this work is towards the development of flexible spine for a quadruped robot. The main contributions of the thesis are in the area of development of an optimization approach to the development of the flexible spine and hardware to validate the design of quadruped robot with a flexible torso. Specific contributions of this work are as follows:

- Development of a simple approach to pseudo-rigid modeling of a continuous beam.
- An optimization scheme to develop an articulated spine-like structure with different boundary conditions under discrete and periodic loading.
- Designing a hardware to act as a flexible multi-segment spine with desired properties. The developed hardware allows the user to make modifications to the shape of the spine after manufacturing. Easy to replace and manufacture, without any moving parts and modular, the structure developed provides a unique way provide multi-degree freedom in the spine.

1.5 Preview

The organization of the thesis is as follows: In chapter 2, the idea and the result of simple transformation between pseudo-rigid-body and a continuous beam are discussed. Chapter 3 describes the optimization problems developed to obtain an articulated spine-like structure for a quadruped robot. This chapter also provides an analysis of the optimized structure under static and dynamic loading. Chapter 4 presents the details regarding the prototype simulation, design, and control. Finally, Chapter 5 provides the conclusions and future directions for the future work.

Chapter 2

Continuous to discrete modeling: a simple approach

2.1 Introduction

Pseudo rigid models are an excellent way to mimic the behavior of a continuous body system. Work done by Howell and Midha [15], Su[16] cover this topic to a great extent. However, these works also raise a few questions. First, all these cases had a clear view of the trajectory of the end point of a cantilever. So is it a must to have a complete set of FEM solution for development of pseudo-rigid-body? Second, what would happen the number of links chosen is greater than 4? Third, The effect of various boundary conditions on the pseudo rigid modeling.

In this chapter, we developed a multi-link pseudo-rigid model for small deflection of a beam and the analyze the effect under different boundary condition on the modeling procedure.

2.2 Mathematical model

The mathematical model of a pseudo-rigid beam is made up of rigid links and joints with springs. We determine a simple approach to obtain the number of links and the stiffness at the joints for a known deflection at a point. The pseudo-rigid-body model is compared with a standard finite element analysis based approach, and it is shown that we can obtain the pseudo-rigid-body approximation with reasonably small errors. It may be mentioned that we assume small deflection.

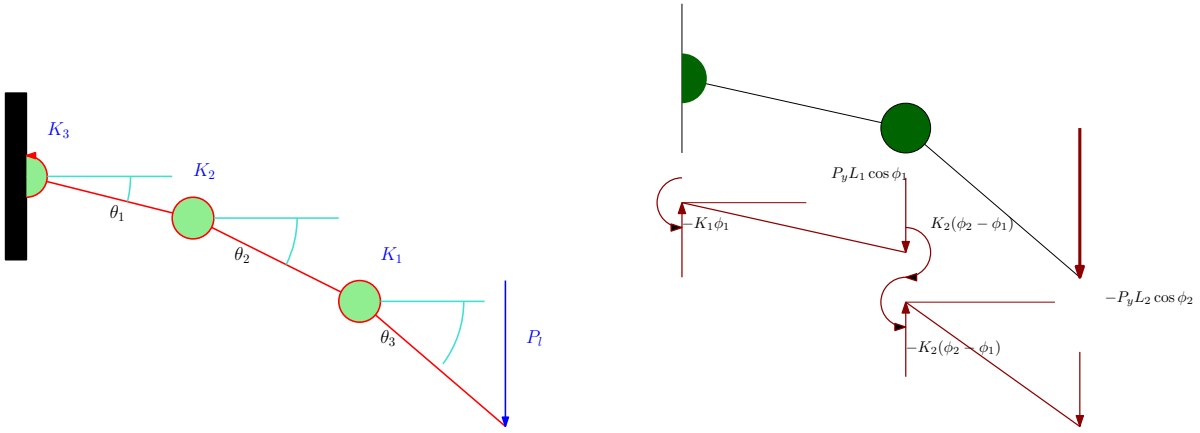

(a) Lumped model of a cantilever

(b) Free body diagram of two interacting link

Figure 2.1: Lumped modeling of a cantilever and Free body diagram

2.2.1 Pseudo rigid modeling of a cantilever

Figure 2.1 shows a cantilever discretized with three rigid links with an end load P. For a cantilever beam, we assume,

1. All link lengths are equal.
2. All the stiffness other than those at the boundary are equal. This is done to simulate the homogeneous nature of the structure.

Under these assumptions, we now discuss the algorithm to transform a continuous cantilever beam int a pseudo-rigid model.

1. Maximum deflection is determined, and with its help, the equivalent stiffness is determined(K_{eq}).
2. The desired stiffness is provided by the user, and α is calculated.
3. The boundary stiffness(K_b) and endpoint stiffness(K_e) is provided. Using these, γ and σ is determined.
4. The following equation is used to determine the number of links so that the deflection at the end remains unchanged.

$$\sigma n^4+(4+4\sigma\gamma-4\sigma-12\alpha\sigma)n^3+(-12\alpha\sigma\gamma-12\alpha-6+12\alpha\sigma+5\sigma-6\sigma\gamma+12\gamma)n^2+(2\gamma\sigma-2\sigma+2)n=0 \quad (2.1)$$

$$K_{eq}=\frac{2E_mI}{L};\ \alpha=\frac{K_d}{K_{eq}};\ \gamma=\frac{K_d}{K_b};\ \sigma=\frac{K_e}{K_d};$$

Where, K_d is the prescribed torsional stiffness, K_e is the torsional stiffness at the end point, K_b is the torsional stiffness at the boundary.

The number of link obtained is a fractional value. But in practice that is not possible. So links are rounded up to their closest integer value and the desired stiffness(K_d) is determined for that integer value using eq. (2.2).

$$K_d = K_{eq}\frac{\frac{\sigma}{12}n^4 + \frac{1+\sigma\gamma-\sigma}{3}n^3 + \frac{5\sigma-6\gamma\sigma+12\gamma-6}{12}n^2 + \frac{\gamma\sigma-\sigma+1}{6}n}{(\sigma n+\sigma\gamma+1-\sigma)n^2} \tag{2.2}$$

The origin of eq. (2.1) and eq. (2.2) has been discussed in appendix C. Equation (2.1) is a fourth order polynomial hence it will have 4 roots. However apart from one root all the others tends to be zero or imaginary. The observation of the solution gives us a linear relationship between the K_d and link number (n), for a given end point deflection and boundary conditions,fig. 2.2.

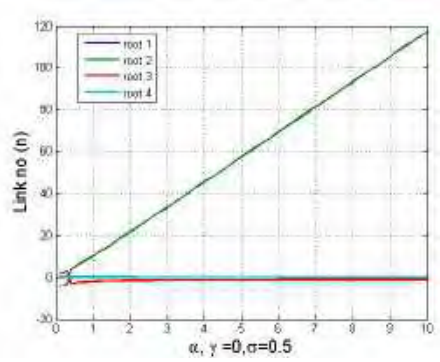

Figure 2.2: Solution of eq. (2.1) for various α

The solution of equation (2.1) under two different boundary condition, fixed end and a spring loaded end, is provided in fig. 2.3(a) and fig. 2.3(b). Each of the figures shows the solution for multiple end conditions.

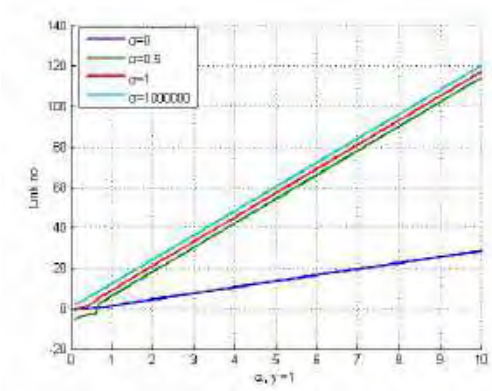

(a) Cantilever with a spring loaded base

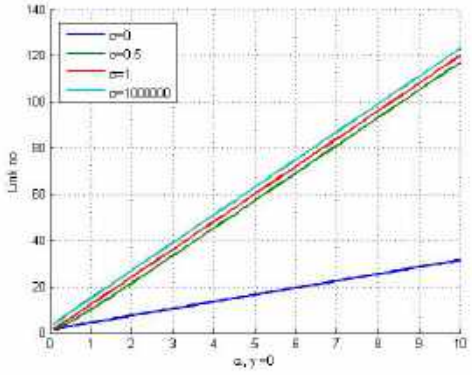

(b) Cantilever with a fixed base

Figure 2.3: Solution of the polynomial under different conditions

2.2.2 Pseudo rigid body model of a beam with both end free

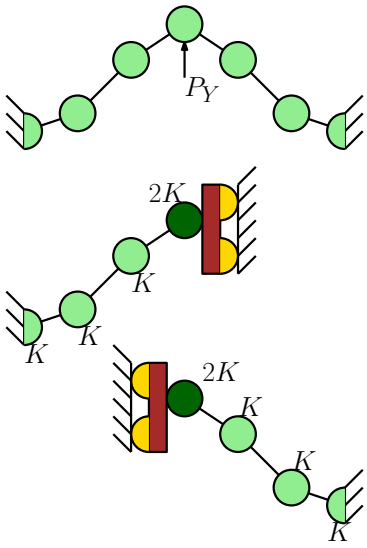

Figure 2.4: Splitting a single beam into two cantilevers.

In this section, we will extend the idea of the pseudo rigid modeling from cantilever to beams with supports at both ends. To derive the pseudo rigid model, we first split the beam into two cantilevers on the point of maximum deflection, fig. 2.4. The point of the division now becomes boundary for the cantilevers and the nodal stiffness there is considered as the boundary stiffness (K_b). It is two times the desired stiffness (K_d). Since the supports were free, the end stiffness (K_e) is considered to be zero. The assumptions in section 2.2.1 and eq. (2.1) are used to derive the number of links required for the pseudo rigid model. In eq. (2.1), σ is set to be 0 and γ is set 0.5.

2.2.3 Pseudo rigid body model of a beam with both end fixed

The process to determine the pseudo rigid model for beams with both ends fixed is similar to free end, but with one key difference. Here, the end stiffness is considered to be very high, usually 10^6 times. Hence in eq. (2.1), σ is set to be 10^6 and γ is set 0.5.

Due to the nature of the eq. (2.1), γ and σ can be interchanged with certain transformation. If point of devision is considered to be the end point rather than the base then γ is 10^{-6} and σ is 2. In both the cases the solution is same.

2.3 Results and discussion

In this section, we discuss the results obtained the formulations from the mathematical models. The results obtained from eq. (2.1) is used decide the number of links and the nodal stiffness of the lumped

multi-body system. The system is then loaded with a prescribed force/moment, and the final deformed structure is recorded.

Next, we compare these results with the results obtained from a standard linear finite element analysis under the same external loading and geometric constraints. For the simulation, we have used 100 one dimensional elements on a 2m long slender beam[1]. The Young's modulus is 2.1GPa, the width of the rectangular cross-section is 10cm and the height is 10cm. Initially, all the beams are kept horizontal. For the cantilever, the load is applied at the very end of the beam. For the supported beams, the load is applied at the middle. Figure 2.5 describes the pseudo rigid model designed from the results obtain

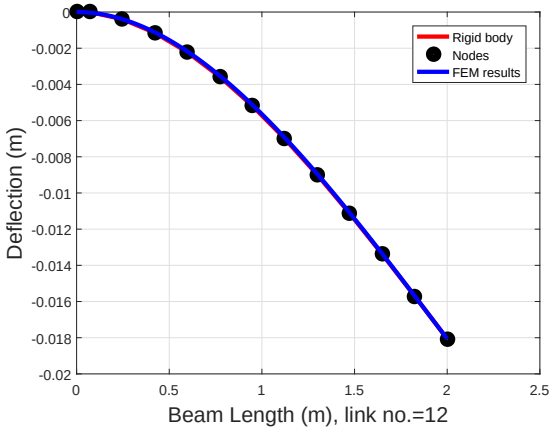

Figure 2.5: Pseudo rigid solution obtained from the formulation

from eq. (2.1) and eq. (2.2). In the same figure we also compare the results to a finite element solution. The error are less than 0.1 %.

In fig. 2.6, a 2m long fixed-fixed beam of width 10cm and height 10 cm is described. A vertical load of $1000N$ is applied at the middle of this beam. the Young's modulus of the beam is 2.1GPa. Similar to the cantilever we compare it with the finite element solution(blue).

In fig. 2.7, a 2m long simple supported beam of width 10cm and height 10 cm is described. A vertical load of $1000N$ is applied at the middle of this beam and the solution is compared with the finite element solution(blue).

Error due to approximation

Since we are using a very specific loading condition to generate the number of links used in pseudo rigid modeling, the solution produces an error when the loading condition changes. Apart from the change in loading condition, the decrease in the number of links also leads to increase in error. In

[1]Developed by M2D2 Laboratory, Mechanical Engg., IISc, Bangalore

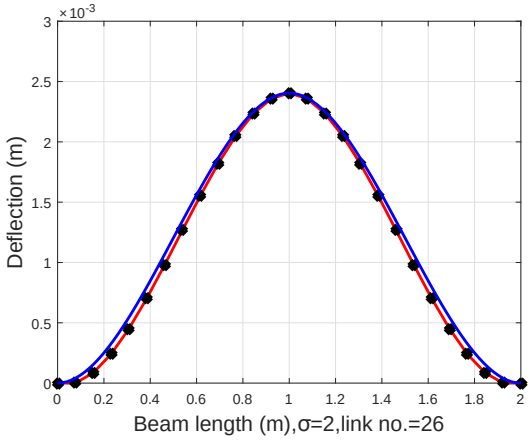

Figure 2.6: Beam with both end fixed

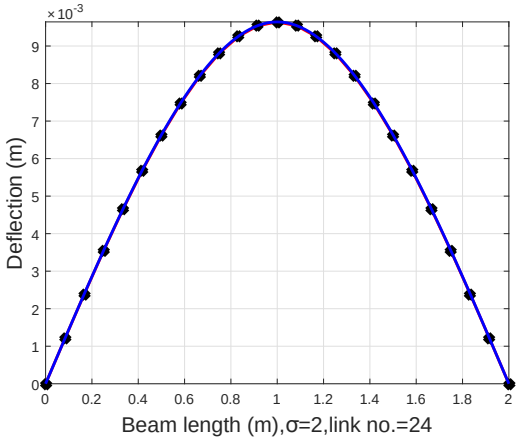

Figure 2.7: Simple supported beam

fig. 2.9 variation of error with the increase in the number of links is described. In fig. 2.10, the loading condition is changed from endpoint external force to endpoint external moment. Figure 2.10(c) describes how the error changes with an increase in the number of links.

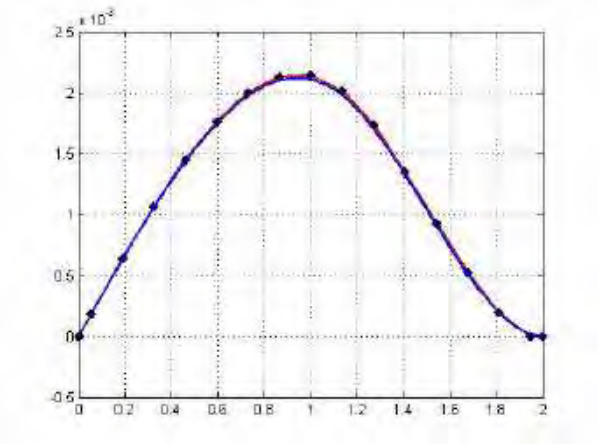

Figure 2.8: Beam with one end free and other end free

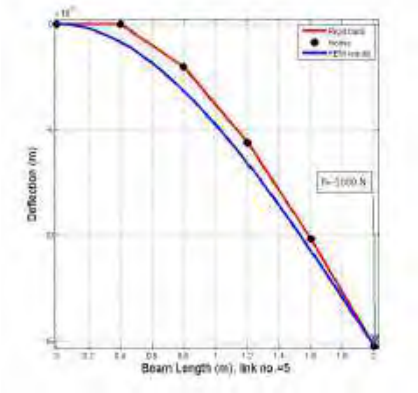

(a) Cantilever deflection and pseudo rigid modelling

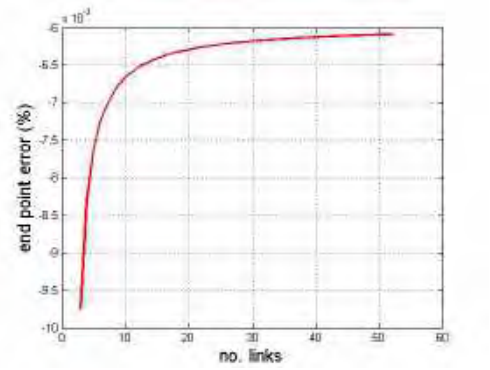

(b) Change in error with the variation of the number of links

Figure 2.9

2.4 Summary

In section, we derived a mathematical formulation for designing n-link pseudo rigid model from continuous beam and compared the results obtained from this model to standard finite element method. We also describe how the error discovered during comparison and how the link number affects it.
The lumped pseudo rigid modeling provides us with the notion that continuous beams can be made into lumped parameters models. Under this notion we extend the ideas to structural optimization. The pseudo rigid model helped us to identify the parameters, link number, nodal stiffness, link length to be used as optimization variable for the optimization problem.

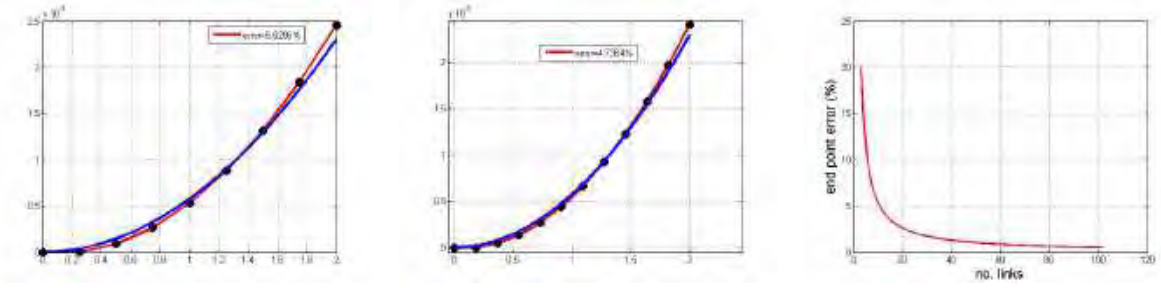

(a) Error generated in a 8 link model (b) Error generated in a 11 link system (c) Behavior of the error due to change in loading type

Figure 2.10: Error generated due to the change in loading type, 100 N-m moment is applied at the end node

Chapter 3

Optimization scheme for spine like structure

3.1 Introduction

The spine or the vertebrae column in an animal is a flexible multi-body structure with multiple degrees of freedom (DoF) at each joint. These joints are actuated and constrained by many muscles and tendons leading to a limited motion of the spine. A one-dimensional serial chain connected by more than three joints, moving in a plane, can be thought of as a hyper-redundant serial manipulator [17]. If the end of such a hyper-redundant serial robot is given a desired displacement, then there exists an infinite number of solutions for the joint variables to achieve the end displacement. To find an unique solution, also called the resolution of redundancy [18], there exists several approaches. All these approaches deal with position and/or velocity of the rigid segment and not with the response to an external loading. In the statics of serial manipulators or a hyper-redundant manipulator, the issue of redundancy does not arise. For a given external force and/or moment applied at the end-effector, the reaction torques or the applied torque at the joints can be obtained from the transpose of the manipulator Jacobian matrix [19]. However, for a given prescribed end-effector motion together with external loading at the joints or at the end, the joint torques cannot be obtained uniquely for a hyper-redundant manipulator. This is because the Jacobian depends on the configuration of the manipulator that is to be determined.

The spine under external loading can be treated as a loaded multi-body serial manipulator with a constrained end-point motion. The equations of motion of a serial manipulator, redundant or otherwise, can be formulated and solved numerically. From this formulation, for a given torque at the joints, the motion of the links can be obtained and likewise the torque at the joints can be computed for a desired motion of the links. In our one-dimensional model, the muscles and tendons of the original

spine are approximated by torsional springs rather than actuators. As none of the joints are active, with the introduction of torsional springs at the joints, the hyper redundant manipulator problem becomes a problem of an under-actuated system [20]. Obtaining the desired motion of an under-actuated serial robot and its shape, when subjected to transverse and axial loading, is much more difficult. In the case of a flexible spine, the model contains a large number of rigid segments to obtain realistic motion. As we do not introduce any actuators capable of directly controlling the states of the system, it can be described as an articulated passive system. The primary reason for this effort, when compared with a spine of a single rigid segment, is that the flexible central structure is known to be more energy efficient [21, 22, 23]. It also known to enable a higher average speed as compared to a rigid central frame. Work done by Khormoashiha and Ijspeert [7] shows the benefits of an active spine. It is clear from this work that the larger the spine deflection the better the average gait speed.

Obtaining the shape of a flexible structure subjected to loading or an end-point displacement and or force is also dealt in the context of shape optimization in compliant mechanisms (see, for example, the work by Xu and Ananthasuresh [13] and the references contained therein). In these studies, the flexible links are modeled as continuous beams and a finite element formulation is used to determine the shape of the structure against external loading and desired deflection. In reference [13], the parameters of Bezier curve have been used as the design variables. A modified version of the work has been done by Zhou and Ting [14] where they have used wide curves to take into account the variable width-profile of the beams. In the case of the spine, the assumption of discrete rigid segments connected by joints is more reasonable and the motion of the rigid segments and the rotations at the joints can be large resulting in significant change in their orientation.

In this chapter, we focus on modeling and design of flexible spines that can bear loads transverse to its axis and also deform in a desired manner due to a load applied along the axial direction. We have used the equation of motion to study the motion of a serial chain of rigid segments connected by joints with torsional springs and damping at the joints. The theory developed is applicable to an arbitrary number of segments. We assume reasonable constraints on the angular motion at the joints. For a given transverse loading, the spring stiffness and link orientation at the joints are obtained by optimizing an appropriate objective functions related to the work done by the loads. Next, for a desired end-point motion, we use a modified objective function and techniques from structural optimization [12] to obtain a design which is not only is capable of bearing transverse loads but also provide the desired end-point motion. Additionally, we attempt to design the flexible structure to give a desired time response by obtaining appropriate damping at the joints. The designs are obtained using a gradient-based optimization techniques.

The chapter is organized as follows: In Section 3.2, we briefly describe the modeling of the flexible one-dimensional spine as a serial chain manipulator, and then derive the equations of motion including

the effect of the springs and dampers at the joints, external loads acting on the nodes and the axial force applied at the free end. In Section 3.3, we analyze the optimization problem for a serial chain with two links and present the necessity of using an optimization approach for a system with large number of links. In Section 3.4, we frame the optimization problems for the static deflection and the dynamic response. In Section 3.5, we describe the numerical methods used to solve the optimization problems and present numerical results for the static and dynamic cases. We are able to show that many of the structures obtained from optimization have similar features to that of the vertebrae of fast moving quadrupeds. In Section 5.1, we present the conclusions, limitations and scope for further work.

3.2 Modeling of a multi-link flexible serial chain

Modeling and analysis of animal spine has become a focus of many research efforts related to locomotion [24, 25]. A realistic view of the vertebrae column would require each segment to have all six degrees-of-freedom (DoF) at each joint if the constraints due to the muscles and tendons are ignored [26]. However, this is computationally intensive. Furthermore, many of the DoFs in the 6-DoF model are unnecessary. To simplify our modeling, we consider the spine to be a multi-body serial manipulator with rigid segments and joints with some limits to the angle of rotations at the joints. We also assume that the joints have torsional springs that offer resistance to the rotations at the joints. Figure 3.1 shows a N link serial chain with one end fixed and the free end subjected to a horizontal force resulting in a desired end motion. The rotations at the joints, θ_i, are with respect to a horizontal X axis and hence are absolute rotations. Each joint has an associated lumped stiffness K_i and a lumped damping C_i. At each joint, there is a loading along the negative Y axis denoted by P_Y which the structure must be capable of bearing in addition to the self-weight. The desired end motion is denoted by δ_X and this is due to a horizontal actuating force P_X. We have no control over the given axial force.

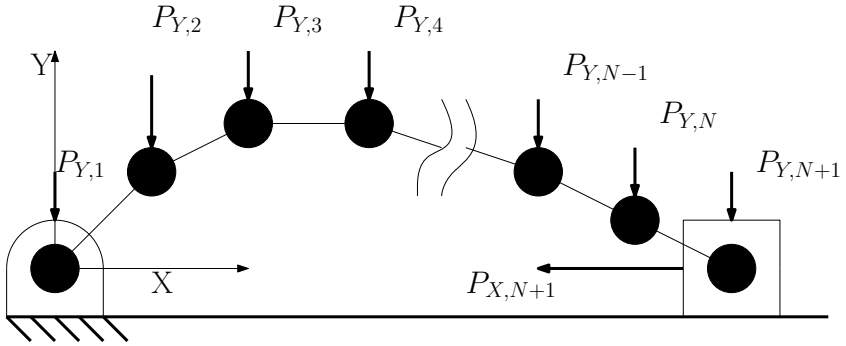

Figure 3.1: An N link constrained serial chain with axial and transverse loading

3.2.1 Equilibrium equation and equations of motion

The location of each joint (X_i, Y_i) is given by

$$X_i = \sum_{j=1}^{i-1} L_j \cos\theta_j, \quad Y_i = \sum_{j=1}^{i-1} L_j \sin\theta_j \tag{3.1}$$

The Y deflection of the end-point is assumed to be zero and hence there exists a constraint, denoted by $\Phi(\theta)$, of the form

$$\Phi(\theta) = \sum_{i=1}^{N} L_i \sin\theta_i = 0 \tag{3.2}$$

Denoting the deflection at the i^{th} joint along X and Y axes by ΔX_i and ΔY_i, respectively and rotation by $\delta\theta_i$, we can obtain the total potential energy as

$$PE = \frac{1}{2}\sum_{i=1}^{N} K_i \delta\theta_i^2 - \sum_{i=1}^{N+1} P_{X,i}\Delta X_i - \sum_{i=1}^{N+1} P_{Y,i}\Delta Y_i - \sum_{k=1}^{N} m_k g Y_{gk} \tag{3.3}$$

where, $\delta\theta_i = (\theta_i - \theta_{0,i}) - (\theta_{i-1} - \theta_{i-1,0})$, $\theta_{0,i}$ is the original orientation of the i^{th} angle, θ_i is the deformed orientation of the i^{th} angle, K_i is the torsional stiffness of the i^{th} joint, L_i is the length of the i^{th} link, $P_{X,i}$, $P_{Y,i}$ are the loads applied along X and Y axis on the i^{th} joint respectively, g is acceleration due to gravity and Y_{gk} is the position of the center of mass of the k^{th} link with mass m_k.

Associating a Lagrange multiplier λ with the constraint in equation (3.2), we can write the Lagrangian

$$\mathcal{L} \quad = \quad -PE + \lambda\Phi(\theta) \tag{3.4}$$

and we can generate $N+1$ equilibrium equations by taking partial derivative with respect to states θ_i and co-state λ. We get,

$$\mathbf{K}_m \delta\theta = \mathcal{P}(\theta) \tag{3.5}$$

where, $\mathcal{P}(\theta)$ denotes the load vector generated due to loadings and constraints.

For a dynamic system we use the Lagrangian ($KE - PE$) and Lagrange multiplier (Λ) with the constraint equation, to develop the equations of motion. Following the standard approach [19], the equations of motion can be written as

$$M_A(\theta)\ddot{\alpha} + C_A(\theta, \dot{\theta})\dot{\alpha} + K_A\delta\alpha = \mathcal{P}(\theta, t) \tag{3.6}$$

where, α is $[\theta\ \Lambda]^T$ with Λ denoting the Lagrange multiplier, $M_A(\theta)$ is the augmented mass matrix, C_A is the matrix of Coriolis and damping terms, $\mathcal{P}$ is the moment vector due to loadings and constraints.

The above equilibrium equations and the equation of motion determine final states when a loading is applied. These equations will be considered as a constraint for the optimization problems discussed in Section 3.4.

3.3 Analysis of the multi-link system

As mentioned earlier, the aim of this work is to design a flexible structure to withstand transverse loads and have a desired motion due to an axial load. To get an insight into the problem, we begin with a simple two-segment system as shown in Figure 3.2. For deriving the mathematical expression we consider the following conventions: $\theta_{0,i}$ is the unloaded orientation of the i^{th} link, $\theta_{1,i}$ is the orientation of the i^{th} link when only the vertical loading is applied, $\theta_{2,i}$ denotes the orientation of the i^{th} link when both vertical and horizontal loading is applied. Additionally, we remove the two springs at joint 1 and

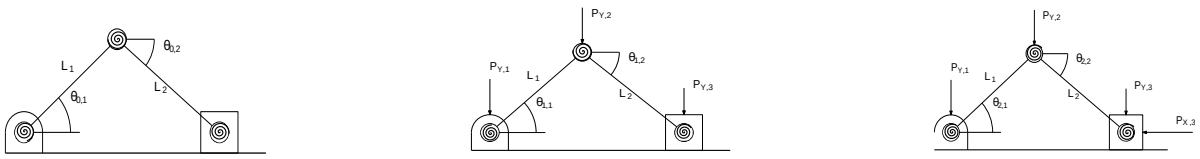

(a) The unloaded structure expressed in general form

(b) Structure loaded by the passive loading, P_Y

(c) Loaded structure with the horizontal force P_X

Figure 3.2: 2 link system with flexible node

3 and consider the two link system with only one torsional spring at the second joint with a spring stiffness denoted by K. The second joint is a also loaded with a vertical force P_Y. It is prescribed that the system deflect by δ along X-axis under the action of an actuating force P_X. The link lengths are assumed to be equal and hence, $\theta_{j,1} = -\theta_{j,2} = \theta_j$. We wish to determine the undeformed angle θ_0 such that for the given nodal stiffness, K, the end point deflection due to the loading P_X is δ.

The static equilibrium equation for the loading conditions is given by

$$4K(\theta_1 - \theta_0) = P_Y L \cos\theta_1 \tag{3.7}$$

$$4K(\theta_2 - \theta_0) = -2P_X L \sin\theta_2 + P_Y L \cos\theta_2. \tag{3.8}$$

The end point deflection by δ can be expressed as $L(\cos\theta_{2,1} - \cos\theta_{0,1}) + L(\cos\theta_{2,2} - \cos\theta_{0,2})$ and since $\theta_{2,1} = -\theta_{2,2} = \theta_2$, we get

$$\cos\theta_2 = \cos\theta_0 + \frac{\delta}{2L}. \tag{3.9}$$

For a given small δ, equations (3.8) and (3.9) can be solved in closed-form to give θ_0 in terms of K as

$$\theta_0 = \frac{1}{2}\left[\sin^{-1}\left(\frac{2P_X - \dfrac{4K\delta}{L^2}}{\sqrt{P_Y^2 + 4P_X^2}}\right) - \tan^{-1}\left(\frac{2P_X}{P_Y}\right)\right] \tag{3.10}$$

Likewise we can obtain an expression for K in terms of θ_0 as

$$K = \frac{L}{2\delta}\left(2P_X L\sin^2\theta_0 - P_Y L\sin\theta_0\cos\theta_0 - \frac{\delta}{2L}\left[2P_X L\cos\theta_0 + P_Y L\sin\theta_0\right]\right) \tag{3.11}$$

For large δ, closed-form expressions are not available and equations (3.8) and (3.9) need to be solved simultaneously using numerical techniques.

The two equations (3.8) and (3.9) are in terms of three variables θ_0, K and δ and there exists infinitely many solutions for these three variables for a given loading P_X and P_Y. This feature makes the problem amenable to optimization of an objective function and we use the minimization of the strain energy stored in the system to obtain an unique solution. We assume that the energy stored in the system is minimum under zero axial loading, i.e., when P_X=0. We pose the optimization problem as follows.

$$\begin{aligned} &\min_{\theta_0, K} && \mathcal{J} = 2K(\theta_1 - \theta_0)^2 \\ &\text{Subject to} && \cos\theta_2 = \cos\theta_0 + \frac{\delta}{2L} \end{aligned} \tag{3.12}$$

where θ_1 is the deflected angle obtained from equation (3.8) under P_Y loading, θ_2 is the deflected angle obtained from equation (3.8) under loading P_X and θ_0 is the undeformed angle.

From the objective function $\mathcal{J} = 2K(\theta_1 - \theta_0)^2$, we can obtain

$$\frac{d\mathcal{J}}{dK} = 2(\theta_1 - \theta_0)^2 + 4K(\theta_1 - \theta_0)\frac{d\theta_1}{dK} \tag{3.13}$$

$$\frac{d\mathcal{J}}{d\theta_0} = 4K(\theta_1 - \theta_0)\left(\frac{d\theta_1}{d\theta_0} - 1\right) \tag{3.14}$$

From equation (3.7), we get

$$\begin{aligned} \frac{d\theta_1}{dK} &= -\frac{4(\theta_1 - \theta_0)}{4K + P_Y L\sin\theta_1} \\ \frac{d\theta_1}{d\theta_0} &= \frac{4K}{4K + P_Y L\sin\theta_1} \end{aligned} \tag{3.15}$$

and substituting the above in equation (3.13) we get

$$\begin{aligned}\frac{d\mathcal{J}}{dK} &= 2(\theta_1-\theta_0)^2\left(1-\frac{2P_Y L\sin\theta_1}{4K+P_Y L\sin\theta_1}\right)\\ \frac{d\mathcal{J}}{d\theta_0} &= 4K(\theta_1-\theta_0)\left(\frac{-P_Y L\sin\theta_1}{4K+P_Y L\sin\theta_1}\right)\end{aligned} \tag{3.16}$$

and finally we can find the ratio of the percentage change in $\mathcal{J}$ with respect to K and θ_0 as

$$R=\frac{2K}{\cot\theta_1+2(\theta_1-\theta_0)} \tag{3.17}$$

Since $K >> 1$ and as long as θ_1 is not close to zero, R is greater than 1. From this we can conclude that the objective function is more sensitive to change in θ_0 in comparison to change in K and change in shape is preferred to change in stiffness. The negative sign implies than increase in K decreases θ_1. The preference of shape over stiffness was also seen in the numerical simulations when there are large numbers of rigid segments. We also use this observation to define a scaling C_K for the general multi-link case discussed later.

The constrained Lagrangian can be written as

$$\mathcal{L}=\mathcal{J}+\lambda_1\left(\cos\theta_2-\cos\theta_0-\frac{\delta}{2L}\right). \tag{3.18}$$

where λ_1 is the Lagrange multiplier. The gradients with respect to the design variables can be written as

$$\frac{d\mathcal{L}}{dK} = 2(\theta_1-\theta_0)^2+4K(\theta_1-\theta_0)\frac{d\theta_1}{dK}-\Lambda_1\sin\theta_2\frac{d\theta_2}{dK} \tag{3.19}$$

$$\frac{d\mathcal{L}}{d\theta_0} = 4K(\theta_1-\theta_0)\left(\frac{d\theta_1}{d\theta_0}-1\right)+\Lambda_1\left(-\sin\theta_2\frac{d\theta_2}{d\theta_0}+\sin\theta_0\right) \tag{3.20}$$

where the derivatives are obtained from equation (3.8) under different loading conditions.

As $\theta_1-\theta_0$ in very small hence $(\theta_1-\theta_0)^2$ is less than $\theta_1-\theta_0$. Also, $1\leq K$, making $4K(\theta_1-\theta_0)\geq 2(\theta_1-\theta_0)^2$. From this it can be said that $\frac{d\mathcal{L}}{dK}$ is less than $\frac{d\mathcal{L}}{d\theta_0}$. This means that changing shape is preferred by the system to changing nodal stiffness. This behavior was also observed in many simulations, specially with larger number of links.

General form for multi-link system

The general form of the energy stored in the N link system due to the loading $P_{y,i}$, denoted by $\mathcal{J}$, can be written as

$$\mathcal{J}=\frac{1}{2}\Delta\theta_1^T\mathbf{K}_m\Delta\theta_1 \tag{3.21}$$

where, $\mathbf{K}_m$ denotes the stiffness matrix and $\Delta\theta_1$ denotes the change in angle θ_0 under vertical loading only – the general form for change in angle is $\Delta\theta_k = \theta_k - \theta_0$. where, $\theta_k = [\theta_{k,1} \ ... \ \theta_{k,i} \ ... \ \theta_{k,N}]^T$. The constraints for general formulation are given by

$$\Phi_1 = \sum_{i=1}^{N} L_i \sin\theta_{0,i}, \quad \Phi_2 = \sum_{i=1}^{N} L_i \left(\cos\theta_{2,i} - \cos\theta_{0,i}\right) - \delta$$

where N denotes the number of links.

For the N link system, the Lagrangian, $\mathcal{L}$, can be written as

$$\mathcal{L} = \mathcal{J} + \lambda_1\Phi_1 + \lambda_2\Phi_2, \tag{3.22}$$

The gradient with respect to K_i is given as

$$\frac{d\mathcal{L}}{dK_i} = \frac{1}{2}\Delta\theta_1^T \frac{d\mathbf{K}_m}{dK_i}\Delta\theta_1 + \Delta\theta_1^T\mathbf{K}_m\frac{d\theta_1}{dK_i} - \lambda_2\sum_{j=1}^{N} L_j\sin\theta_{2,j}\frac{d\theta_{2,j}}{dK_i} \tag{3.23}$$

and the gradient with respect to $\theta_{0,i}$ is

$$\frac{d\mathcal{L}}{d\theta_{0,i}} = \Delta\theta_1^T\mathbf{K}_m\left[\frac{d\theta_1}{d\theta_{0,i}} - \frac{d\theta_0}{d\theta_{0,i}}\right] + \lambda_1 L_i\cos\theta_{0,i} - \lambda_2\sum_{j=1}^{N} L_j\sin\theta_{2,j}\frac{d\theta_{2,j}}{d\theta_{0,i}} + \lambda_2 L_i\sin\theta_{0,i} \tag{3.24}$$

The expressions of $\dfrac{d\theta_k}{d\theta_{0,i}}$, $\dfrac{d\theta_k}{dK_i}$, $k = 0, 1, 2$ are given in Appendix A.

For the two link system without K_3, for a small deflection, we get from equations (3.22)

$$\mathbf{K}_m = \begin{bmatrix} K_1 + K_2 & -K_2 \\ -K_2 & K_2 \end{bmatrix}; \tag{3.25}$$

$$\Delta\theta_k = \begin{bmatrix} K_1 + K_2 & -K_2 & L_1\cos\theta_{0,1} \\ -K_2 & K_2 & L_2\cos\theta_{0,2} \\ L_1\cos\theta_{0,1} & L_2\cos\theta_{0,2} & 0 \end{bmatrix}^{-1} \begin{bmatrix} P_{Y,2}L_1\cos\theta_{0,1} - P_{X,3}L_1\sin\theta_{0,1} \\ P_{X,3}L_2\sin\theta_{0,2} \\ -L_1\sin\theta_{0,1} - L_2\sin\theta_{0,2} \end{bmatrix}; \tag{3.26}$$

where, k =1 if $P_{X,3}$ =0, k =0 if $P_{X,3}$ =0 & $P_{Y,2}$ =0 and k =2 if $P_{X,3}$ & $P_{Y,2}$ are non-zero.

For small deflection,

$$\sin\theta_{j,i} = \sin\theta_{0,i} + \cos\theta_{0,i}\Delta\theta_{j,i}; \quad \cos\theta_{j,i} = \cos\theta_{0,i} - \sin\theta_{0,i}\Delta\theta_{j,i};$$

The gradient with respect to K is given as

$$\frac{d\mathcal{L}}{dK_1} = \frac{1}{2}\Delta\theta_{1,1}^2 + \Lambda_1\frac{d\Phi_1}{dK_1} + \Lambda_2\frac{d\Phi_2}{dK_1}; \tag{3.27}$$

$$\frac{d\mathcal{L}}{dK_2} = \frac{1}{2}(\Delta\theta_{1,1} - \Delta\theta_{1,2})^2 + \Lambda_1\frac{d\Phi_1}{dK_2} + \Lambda_2\frac{d\Phi_2}{dK_2}; \tag{3.28}$$

and the gradient with respect to $\theta_{0,i}$ is given as

$$\frac{d\mathcal{L}}{d\theta_{10}} = \Delta\theta^T\mathbf{K}_m\frac{d\theta_1}{d\theta_{10}} - \Delta\theta_1^T\mathbf{K}_m\begin{bmatrix}1\\0\end{bmatrix} + \Lambda_1\frac{d\Phi_1}{d\theta_{0,1}} + \Lambda_2\frac{d\Phi_2}{d\theta_{0,1}}; \tag{3.29}$$

$$\frac{d\mathcal{L}}{d\theta_{20}} = \Delta\theta_1^T\mathbf{K}_m\frac{d\theta_1}{d\theta_{20}} - \Delta\theta_1^T\mathbf{K}_m\begin{bmatrix}0\\1\end{bmatrix} + \Lambda_1\frac{d\Phi_1}{d\theta_{0,2}} + \Lambda_2\frac{d\Phi_2}{d\theta_{0,2}}; \tag{3.30}$$

where,

$$\frac{d\Phi_2}{d\theta_{2,1}} = -L_1\sin\theta_{2,1}; \quad \frac{d\Phi_1}{d\theta_{0,1}} = L_1\cos\theta_{0,1};$$
$$\frac{d\Phi_2}{d\theta_{2,2}} = -L_2\sin\theta_{2,2}; \quad \frac{d\Phi_1}{d\theta_{0,2}} = L_2\cos\theta_{0,2};$$
$$\frac{d\Phi_2}{d\lambda} = 0; \qquad \frac{d\Phi_1}{d\lambda} = 0;$$

To be an optimal solution the equations (3.27) to (3.30) must be equal zero. To normalize the effects of change in stiffness and the shape, we introduce a modified stiffness K_{di}. The relationship between K_{di} and K_i is given by

$$\frac{d\mathcal{L}}{dK_{d1}} = C_K\frac{d\mathcal{L}}{dK_1}, \quad \frac{d\mathcal{L}}{dK_{d2}} = C_K\frac{d\mathcal{L}}{dK_2}$$

where C_K equal to 1 implies there is almost no participation of stiffness in the optimization scheme (for a large number of links) and a large C_K such as 1000 indicate that there is a significant effect of stiffness. The C_K scales the gradients to a comparable values. This allows the two type of variables to change simultaneously.

3.4 Optimization problems

For a multi-link system, there are no closed-form solutions just from the equilibrium equation and constraint equations. To generate an unique solution, we formulate an optimization problem. We follow the the structural optimization approach as shown in Haftka [12] and others and choose an objective function. We assume that the flexible structure must first support its own weight.

To be able to withstand its own weight, the internal strain energy(PE) stored should be minimum due to passive loading, $\mathcal{P}_1(\theta)$. We can write the internal energy stored as follows:

$$PE = \sum_{i=1}^{N+1} \frac{1}{2} K_i(\theta_{1,i-1} - \theta_{0,i-1} - \theta_{1,i} + \theta_{0,i})^2 \tag{3.31}$$

To achieve the desired flexibility we introduce a local constraint under active loading, $\mathcal{P}_2(\theta)$.

$$\sum_{i=1}^{N} L_i(\cos(\theta_{2,i}) - \cos(\theta_{0,i})) - \delta_d = 0. \tag{3.32}$$

The above equation describes the end point deflection to be δ_d if the loading condition on the structure is $\mathcal{P}_2(\theta)$. However, the loading condition $\mathcal{P}_2$ need not be constant with time and it could be a periodic function (as in running). We address this by considering first a constant loading condition and second a periodic loading where, the force changes as a function of time. Against a constant force we solve for the shape and stiffness under statics condition and the time response under dynamic condition. For periodic forces, we solve these two simultaneously.

3.4.1 Optimization problem: Static deflection

The general form for an optimization problem for an arbitrary number of segments can be posed as follows:

$$\begin{aligned}
\min_{\theta_0, K_v} \quad & \mathcal{J} = \frac{1}{2} \sum_{i=1}^{N+1} K_i(\Delta\theta_{1,i} - \Delta\theta_{1,i-1})^2 \\
\text{Subjected to:} \quad & \mathbf{K}_m(\theta_1 - \theta_0) - \mathcal{P}(\theta_1) = 0 \\
& \mathbf{K}_m(\theta_2 - \theta_0) - \mathcal{P}(\theta_2) = 0 \\
& \delta = \sum_{i=1}^{N} L_i(\cos(\theta_{2,i}) - \cos(\theta_{0,i})) \\
& \delta - \delta_d = 0 \\
& L_i = L_{x,i} / \cos\theta_{0,i} \\
\text{Data:} \quad & (K_{initial}, \theta_{initial}, K_{boundary}, L_x, \delta_d)
\end{aligned} \tag{3.33}$$

In the above, K_i are spring stiffness at the joints, $\mathcal{P}(\theta_i)$ denote the loading, L_i are the link lengths, δ_d is the desired end-point deflection along the axial direction and θ_i is the vector of joint angles at i^{th} loading condition. The constraints and ranges on θ_0 and K are based on informed guess work as there no data available for these type of problem from a biological system or a robot (see also Section 3.5).

In Section 3.3 to study the relative effect of stiffness (K) and orientation (θ_0), we had introduced a

factor C_K. In terms of this factor, we can frame the optimization problem as

$$\min_{\theta_0, C_K^{-1}K_v} \quad \mathcal{J} = \frac{1}{2}\sum_{i=1}^{N+1} K_i(\Delta\theta_i - \Delta\theta_{i-1})^2 \tag{3.34}$$

where, C_K is the factor that equalizes stiffness magnitude to the radians. This allows the system to change both the stiffness and orientation simultaneously.

In Section 3.5, we use a gradient based technique to solve the aforementioned optimization problem.

3.4.2 Optimization problem: Dynamic response time

For the dynamic case, we assume a constant actuation at the endpoint and determine the response time of the structure. To remove oscillations within the structure we ensure the structure to be over-damped by adjusting the lower limit of the damping coefficient. To control the time response against the constant loading, we introduce the square of the damping coefficient to be the objective function.

Under large dissipative forces in the system, the end point motion behavior is similar to the equation of $(1 - e^{-\alpha t})$. To control the rise time, we consider a cutoff value[1] from the equilibrium value – we have assumed Δ_{cutoff} as 0.9 times the deflection value at equilibrium, δ_d. The optimization problem for the dynamic case can be framed as

$$\begin{aligned}
\min_{\vec{C_v}} \quad & \frac{\Lambda}{2}\vec{C_v}^T\vec{C_v} \\
\text{Subjected to} \quad & M(\theta)\ddot{\theta} + C(\theta,\dot{\theta})\dot{\theta} + K(\theta - \theta_0) - \mathcal{P}(\theta) = 0 \\
& t|_{\delta=\delta_d} = T_d \\
\text{Data:} \quad & C_{initial}, C_{boundary}, T_d
\end{aligned} \tag{3.35}$$

In the above, C_v denotes the damping and as in the static optimization, we assume reasonable damping – in our simulation we have assumed $1 \leq C_{v,i} \leq 10^3$. The optimization problem in equation (3.35) is solvable because there exists a direct closed-form relationship between the constraints (cut-off time and end point deflection). The end point deflection is given by

$$\begin{aligned}
\delta x(t) &= \delta_d(1 - e^{-\tau t}) \\
\text{where,} \quad \tau &= -\tfrac{1}{T_d}\ln\tfrac{\Delta_{cutoff}}{\delta_d}
\end{aligned} \tag{3.36}$$

Here, $\delta x(t)$ is the end point deflection with time, Δ_{cutoff} is the magnitude deflection corresponding to time T_d. Δ_{cutoff} and T_d are two user prescribed values determine the response time of the end

[1] We use $eventfunction$ is Matlab [27] during numerical simulations.

point motion against a constant loading. The lower limit of the nodal damping is set, through trial and error, to ensure the end point motion will be always a second order over damped motion. To simplify our approach we directly assume the motion to be a 1^{st} order motion and make predictions about the response. This assumptions are backed by numerical results described in Section 3.5.

In a combined static and dynamic optimization case, we consider the forcing function to be periodic with a frequency of $\frac{\Omega}{2\pi}$ Hz. Our objective is to generate a set of parameters of the N link system that will satisfy our demand for a maximum deflection of δ_d while maintaining minimum strain energy under passive loading. The optimization problem can be stated as follows:

$$\begin{aligned}
\min_{K} \quad & \frac{1}{2}\sum_{i=1}^{N+1} K_i(\Delta\theta_{1,i} - \Delta\theta_{1,i-1})^2 \\
\text{Subjected to} \quad & K(\theta_1 - \theta_0) - \mathcal{P}(\theta_1) = 0 \\
& M(\theta_2)\ddot{\theta_2} + C(\theta_2, \dot{\theta}_2)\dot{\theta}_2 + K(\theta_2 - \theta_0) - \mathcal{P}(\theta_2, \Omega t) = 0 \\
& \min\left(\sum_{i=1}^{N} L_i(\cos(\theta_{2,i}) - \cos(\theta_{0,i}))\right) - \delta_d = 0 \\
\text{Data:} \quad & (K_{initial}, \theta_{initial}, K_{boundary})
\end{aligned} \tag{3.37}$$

It can be observed that the above combined optimization problem involves a differential equation (equation of motion) as a constraint. In addition, a constraint involving a minimum is also present. A gradient-based optimization does not yield results if the constraints contain a maximum or minimum value from a series of data and a genetic algorithm or pattern search yields more effective results [31]. We have used genetic algorithm to generate the solution for the combined dynamic problem.

3.5 Numerical methods and results

The optimization problems in equations (3.33) and (3.35) were solved in Matlab [27] using $fmincon$ which is a gradient based optimization procedure. However the optimization problem in equation (3.37) could not be solved using $fmincon$ and we have used genetic algorithm and pattern search. We have used Matlab [27] library function ga and $patternsearch$ for implementing genetic algorithm and pattern search. The length of each link along X-axis are assumed to be equal and given by L_x/N m with L_x as the total length of the flexible spine and N is the number of links. Apart from the constraints described earlier, we list below additional constraints and choices made for the numerical simulations which make the solutions more reasonable.

Geometrical and stiffness values

We have used the following constraints and ranges for the geometrical and stiffness variables in all the numerical simulations.

- Length constraint: $L_i = \dfrac{L_{X,i}}{\cos\theta_{0,i}}$
- Angle constraint: $-\frac{\pi}{6} \leq \theta_{i0} \leq \frac{\pi}{6}$
- Relative angle constraint: $-\frac{\pi}{6} \leq \theta_{0,i} - \theta_{0,i+1} \leq \frac{\pi}{6}$
- Stiffness limit: $10^2 \leq K_i \leq 10^4$
- Geometric upper and lower limit: $0.01 \leq Y_{0,i} \leq 0.25L_x$

The upper and lower bound of the nodal stiffness is based on the study done by Lavaste and Mazel [28]. They state the average approximate torsional stiffness against flexion to be 3 $N-m/deg$ or 172 $N-m/rad$ for spine motion segment. We have used 100 N-m/rad as the lower bounds and 1000 N-m/rad as the upper bound for the stiffness value at the joints. The upper limit of $Y_{0,i}$ is an user prescribed criteria as no such number is available in literature. Like wise the choice lower limit of $Y_{0,i}$ is also arbitrary. The only constraint on the lower limit is to ensure that the Y value is not negative. The initial orientation, $\theta_{0,i}$, is constrained to ensure link length dimension $L_{link} = \dfrac{L_{X,i}}{\cos\theta_{0,i}}$ is reasonable. If $\theta_{0,i}$ is large then the link length can be come very large and we have constrained $\theta_{0,i}$ to be between $\pm\pi/6$. The local orientation, $\theta_{0,i} - \theta_{0,i-1}$, constraint prohibits the structure from generating sharp changes in rotation between two links or form knots when there is a large number of links.

Applied force value selection

To the best of our knowledge there are no estimates for the applied axial force in a moving quadruped robot and likewise in the muscles of a fast moving animal. It is known in literature [29] that for an active young adult male tennis player, the volume of the muscle is approximately 480 cm^3 and in a study done by Akagi and Fukunaga [30], it is mentioned that a 350 cm^3 muscle generates approximately 76 N-m of torque. Dividing this number with the arm length, the force generated by the muscle, at it's peak, is about 310 N of force. In our simulations, we have assumed the axial force, $P_{X,2}(N+1,1)$ as - 400 N. However, any other value could also be used.

3.5.1 Static optimization

The solutions to the optimization for different static loading and different number of rigid segments is presented here. As stated in Section 3.4, the initial angles and the nodal stiffness are considered as the design variables. We solve for the optimal values for 5 and 10 rigid segments. The simulation is

conducted under an uniform vertical loading of -10 N/node for 5 segment system and -5 N/node for the 10 segment system. The horizontal force applied at the end node is -400 N. The initial solution provided for the optimization problem, for 5 link system, is $\{\frac{\pi}{5}$,0,0,0,-$\frac{\pi}{5}$,10000,250,250,250,250,0$\}$. The results of the static optimization problem described in equation (3.12) are shown in figure 3.3.

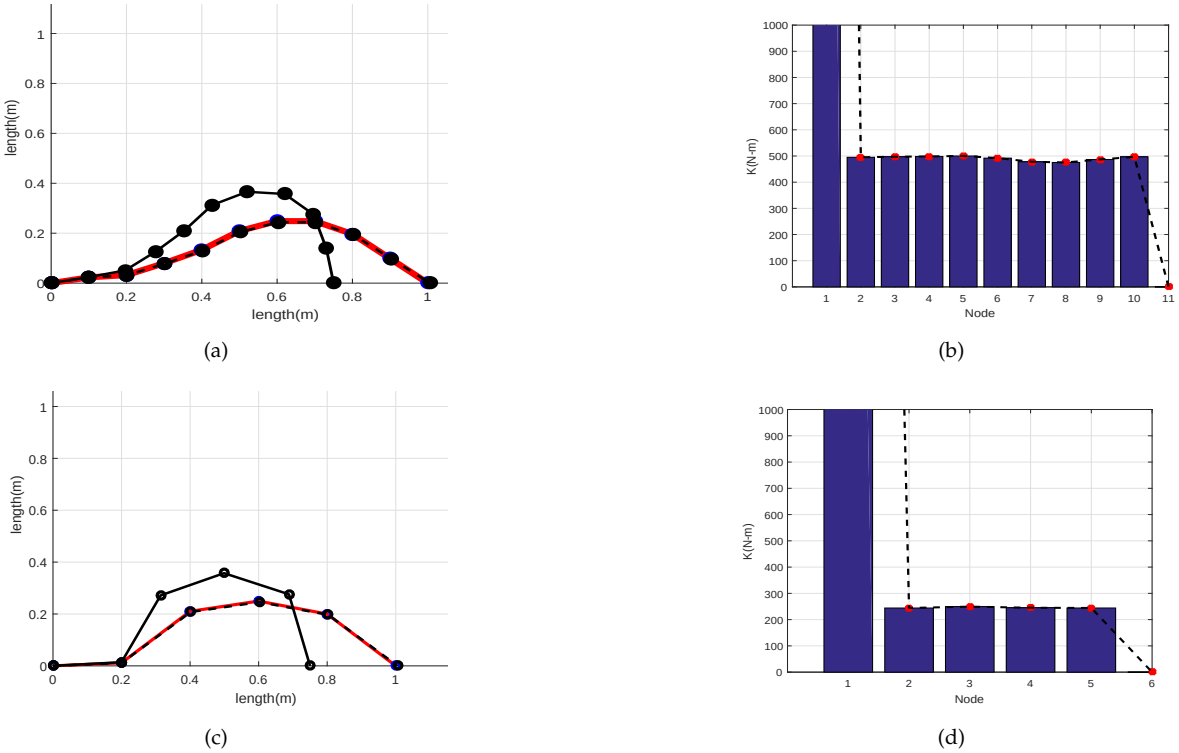

Figure 3.3: (a) undeformed and deformed structure of a 10 segment system, (b)the nodal stiffness of the structure, (c) undeformed and deformed structure of a 5 segment system, (d) the nodal stiffness of the structure

Next, we demonstrate the localized stiffening of the structure and end point motion indifference to the variation of localized loading. The number of rigid segments chosen are 10. The vertical loading at every node from 1 to 5 is -20 N and all other nodes loading force is -5 N. While the horizontal axial loading is -400 N at the end node. The results described in figure 3.4 have similar condition of that described in this problem except the vertical loading is uniform all over the nodes. From the results displayed in figure 3.4, it can be seen by changing the orientation of links of the loaded region the effect of the extra load is mitigated and end effector motion remains unchanged. This validates our claim of "localized stiffening of the structure and end point motion indifference to the variation of localized loading ".

The factor C_K in the optimization problem changes the gradient with respect to the modified nodal stiffness. This is similar to putting a cost on the design parameters. A very high C_K means the cost

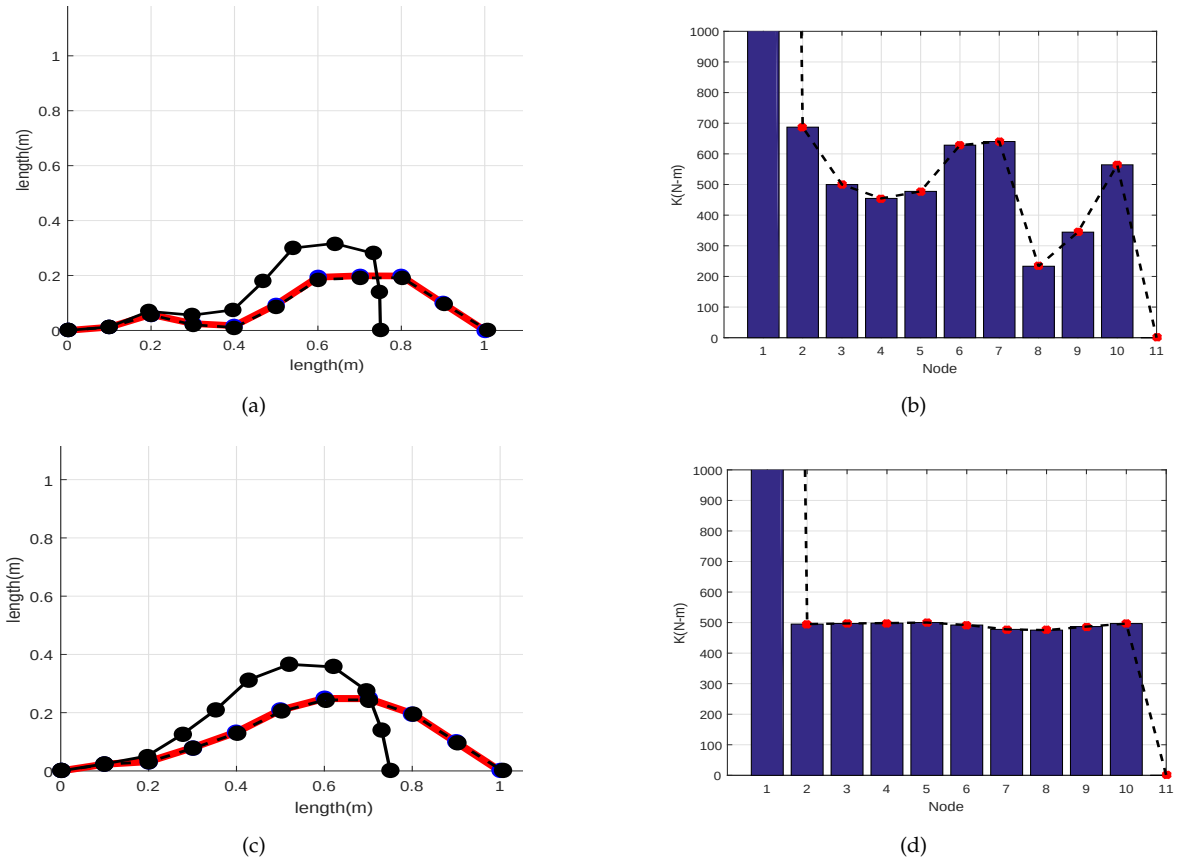

Figure 3.4: (a,b) Node 1 to Node 5, -20 N per node, rest -5 N per node and (c,d) Uniformly loaded with -5 N per node

of changing stiffness is high compared to the cost of changing orientation and vice versa. This idea can be verified by the variation of shape (fig. 3.6(a) to fig. 3.8(a)) and variation of stiffness (fig. 3.6(b) to fig. 3.8(b)). As the C_K is increased the stiffness variation between the nodes increases where as the change in orientation of the links is less apparent.

3.5.2 Dynamics

In this section we describe the results related to the response of the structure for constant and periodic loading. We consider the structures obtained from the static optimization process under the prescribed static loading condition and attempt to control their response time by parameter optimization. Towards the end of this section we show that a structure obtained from static optimization process can also be used with periodic loading if the response time of the structure is fast enough.

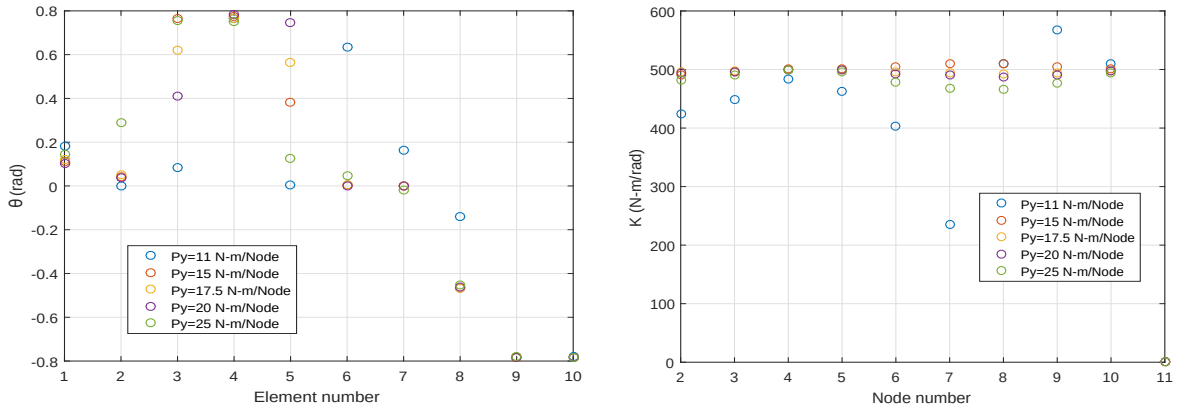

(a) (b)

Figure 3.5: (a) Variation of design variable θ_0 under various loading condition and (b) Variation of design variable $\mathcal{K}$ under various loading condition

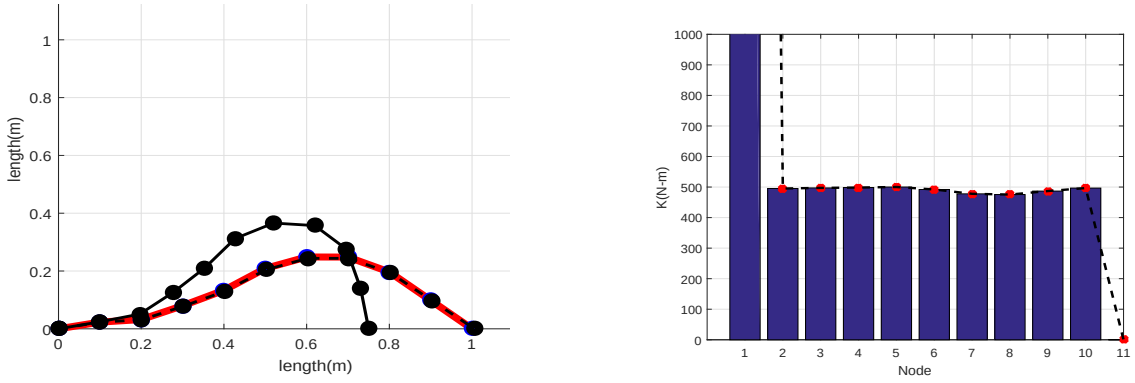

(a) (b)

Figure 3.6: C_K=1, Transverse loading -5N per node, Link no. 10, Axial loading -400 N

Case 1: Application of constant force

In real world scenario the structure deforms over a certain amount of time before it attains equilibrium for a constant force. By adjusting the nodal damping we can predict the response of the structure. The results, figure 3.9, describe the response of a 5-link and a 10-link structure, fixed at one end and free at other, when actuated by a constant force. As it can be seen from equation (3.36) one can predict the response of the structure quite accurately. The time constant of the structure is obtained as $\tau = 11.5$ sec^{-1}.

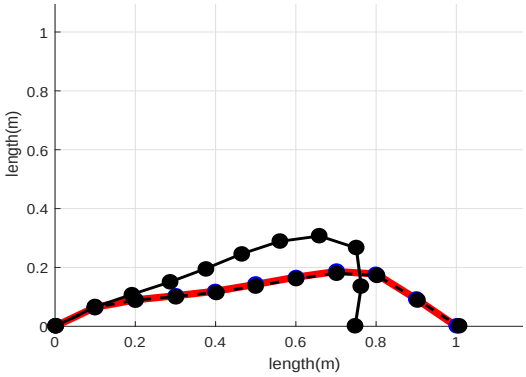

(a)

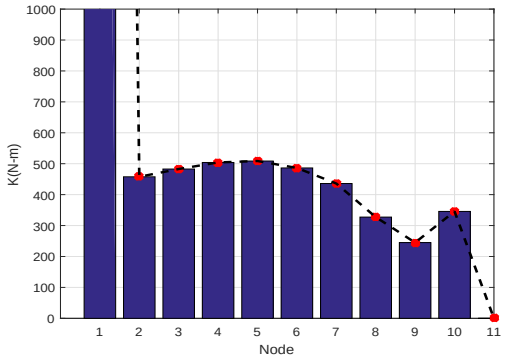

(b)

Figure 3.7: C_K=10^2, Transverse loading -5N per node, Link no. 10, Axial loading -400 N

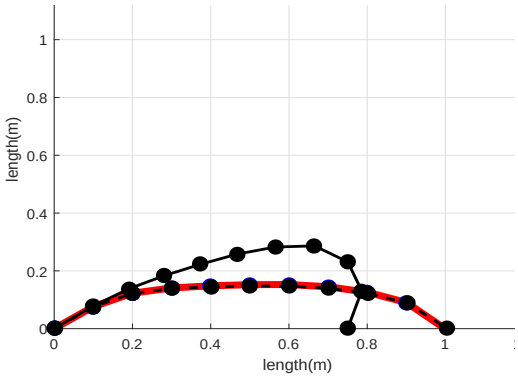

(a)

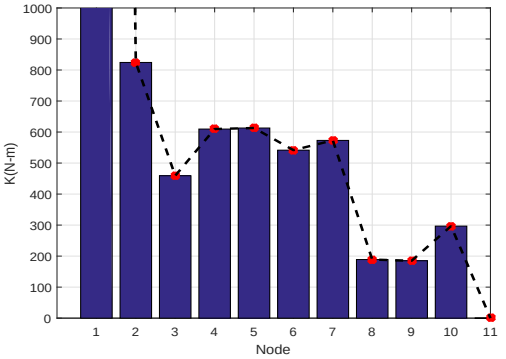

(b)

Figure 3.8: C_K=10^4, Transverse loading -5N per node, Link no. 10, Axial loading -400 N

Case 2: Application of periodic force

We optimize the structure for a periodic end force to simulate rapid and periodic movement of the end point. The number of links chosen for this simulation is 7 and we use a genetic algorithm for optimization in this case. The vertical loading on each node is assumed to be -50 N and from node 2 to 4 it is assumed as -100 N. The horizontal loading is chosen to be -4000 N. We assume the nodal damping as 50 N-m/(rad/s) and mass of the links as 0.5 kg. The results from optimization are shown in figure 3.10. It can be seen that the end-point reaches the desired δ in 0.5 seconds. However, when the load is removed the structure returns to its original state in about 0.25 seconds. This result indicates that the release of stored energy is much faster.

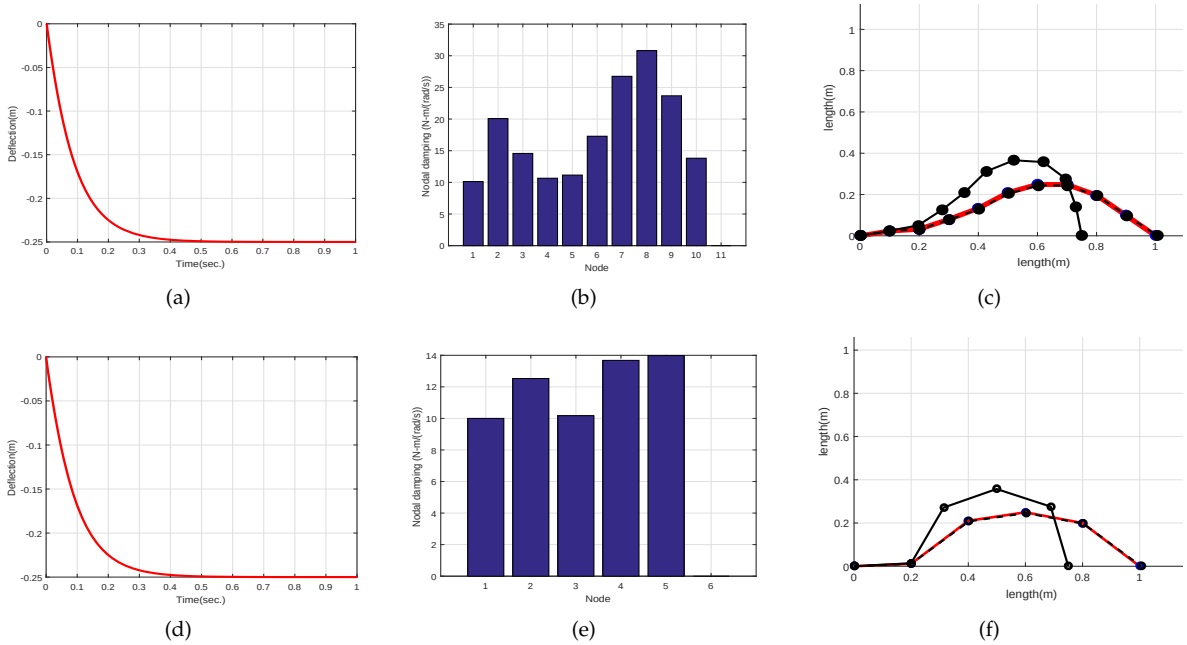

Figure 3.9: (a) End point response of structure with 10 link, (b) Nodal damping of the 10 link system, (c) Undeformed and deformed structure of a 10 link system, (d) End point response of structure with 5 link, (e) Nodal damping of the 5 link system, (f) Undeformed and deformed structure of a 5 link system

Fast responsive constant load solution

Figure 3.11 shows the response of the 10 link structure obtained using gradient based optimization algorithms. Comparing this result with that obtained by genetic algorithm indicates that for a fast-responsive structure, the response at the end point is similar. The gradient based approach is however much faster for simulation.

As can be seen from the figures fast-responsive structure can generate motion as per our requirement even if the actuating force is not constant. This approach is valid only for loading patterns with lower frequency, fig. 3.12. With a small modification in the actuating force application, we can achieve structure supporting fast locomotion with static optimization.

It has been observed from extensive simulations that the general optimization problem, (3.33), is a non-convex system. Thus there are many solutions. Secondly, in all the numerical simulations we have used a chosen set of parameter values based on informed guess work and literature. The gradient based or the genetic algorithm [31] based solution procedure is in no way limited by these choices and can be used for other parameter values.

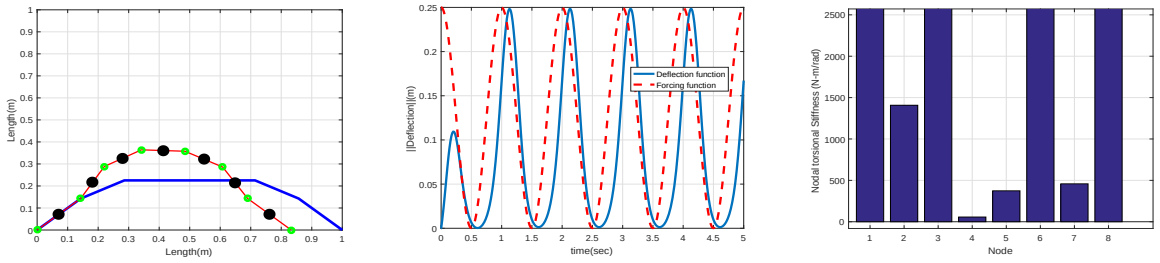

(a) (b) (c)

Figure 3.10: 7 link structure nodal stiffness optimization under dynamic loading

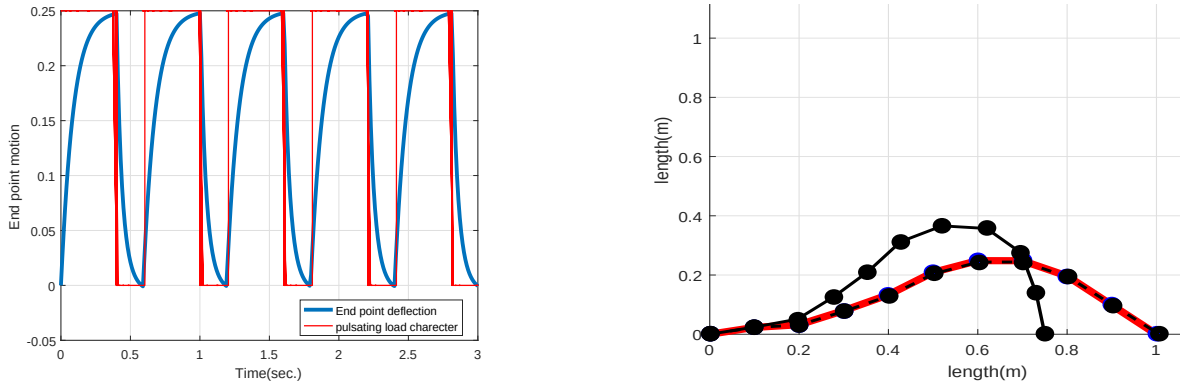

(a) (b)

Figure 3.11: (a) Pulsating oscillation and it's corresponding end point motion, (b) Response of the structure to the oscillation.

3.6 Summary

This chapter deals with the formulation, description and numerical solution of an optimization problem. First we describe why the articulated spine generation should be considered to be an optimization problem. Next, the formulation and solution if the optimization problem provides us with the shape and the stiffness of the spine. The objective function of the optimization problem represents the rigidity and the constraint of optimization problem contains the flexibility. The second optimization provides us with the nodal damping on various parts of the structure, which controls the response time of the spine. Once generated, we test the spine under periodic loading conditions and analyze the end point motion of it.

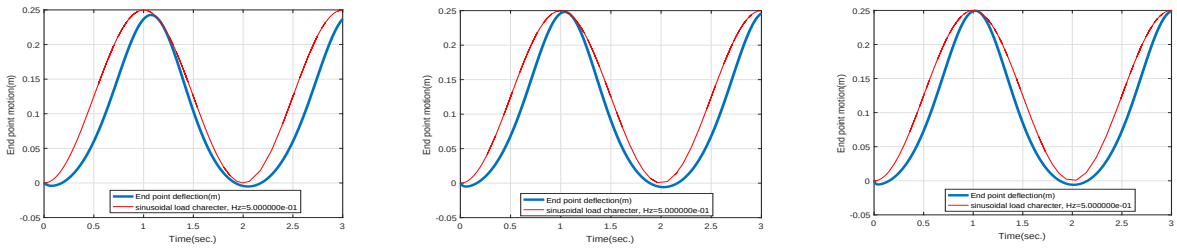

(a) (b) (c)

Figure 3.12: (a) Response time 0.2s for 90% of the maximum deflection, (b) Response time 0.1s for 90% of the maximum deflection, (c) Response time 0.05s for 90% of the maximum deflection.

Chapter 4

Hardware design and experiments

4.1 Introduction

Quadruped robots comes in various forms and features. These features can be classified on the basis of speed of locomotion, fast moving[32, 5] and slow moving quadruped[1]. On the basis of actuation, it can be electrically actuated[34] or pneumatically actuated or hydraulically actuated[1] or on the basis of design they can be bio-inspired or bio-mimetic or some other type of quadruped. For the problems at hand, we are interested in bio-inspired, fast moving quadruped. These types of quadrupeds are mostly operated by electric actuator, rotary or otherwise. The demand for higher efficiency and speed out of a quadruped, is making researchers to look into animal anatomy for answers. For all purposes the cheetah and other fast galloping mammals' anatomy are at the center of these attention. These studies have now set a few standard design feature for fast moving quadrupeds. Robots such as MIT cheetah[5], Cheetah-cub[32], Onichela, etc. have incorporated these features. To develop our own the hardware, we followed the mechanical design and control of these fast motion quadrupeds. During our survey, the approach taken by Alexander Sproiwitz, in the development of cheetah cub, was the most affordable one we came across.

4.2 Design of a Quadruped

Cheetah-cub along with all other fast moving robots have some distinct features. Such as Pantograph style legs, lower leg inertia, compliance in the structure to save energy and shock absorption capacity. In this section these features will be discussed in details along with how they are applied in designing of "Prototype" 1 & 2.

Pantograph leg

Fast running animals have natural shock absorbers and compliance in their legs structure. Pantograph like leg structure is one such design. Nearly all quadruped mammals pose this pantograph like structure. The main benefit of such a design is its ability to absorb impact and store the energy in the compliance attached to it. An open pantograph with a compliant link, as in ASLIP, is able to absorb shock during impact. Te reduced impact causes less energy loss and less strain on the structure of the leg. However, the complicated design of the leg poses a challenge for simulation process. To avoid this

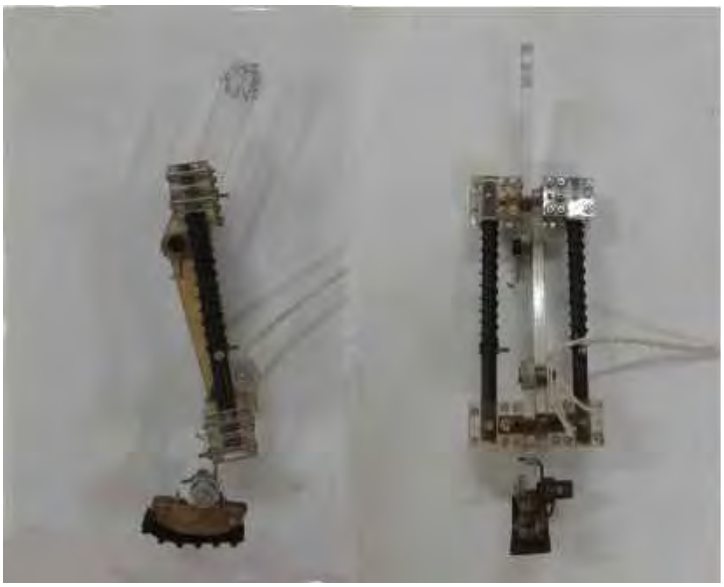

Figure 4.1: Closed pantograph style legs

complication and for the ease of simulation and design, we have used closed pantograph structure in place of open pantograph structure.

Leg design with wire actuation

We previously discussed the advantages of pantograph style leg; now we will discuss methods to reduce over all inertia of the leg to make the motion of the legs faster.

The main contributors to the weight and inertia of the legs are the actuators. To reduce weight, the actuators are placed on the main body. With the help of wire based transmission system the motion of the knee joint is controlled. This mechanism and its physical model is shown in fig. 4.2(a) and fig. 4.2(b) respectively. To avoid the loss of movement, the wire is passes node at the hip, white cover in fig. 4.2(b).

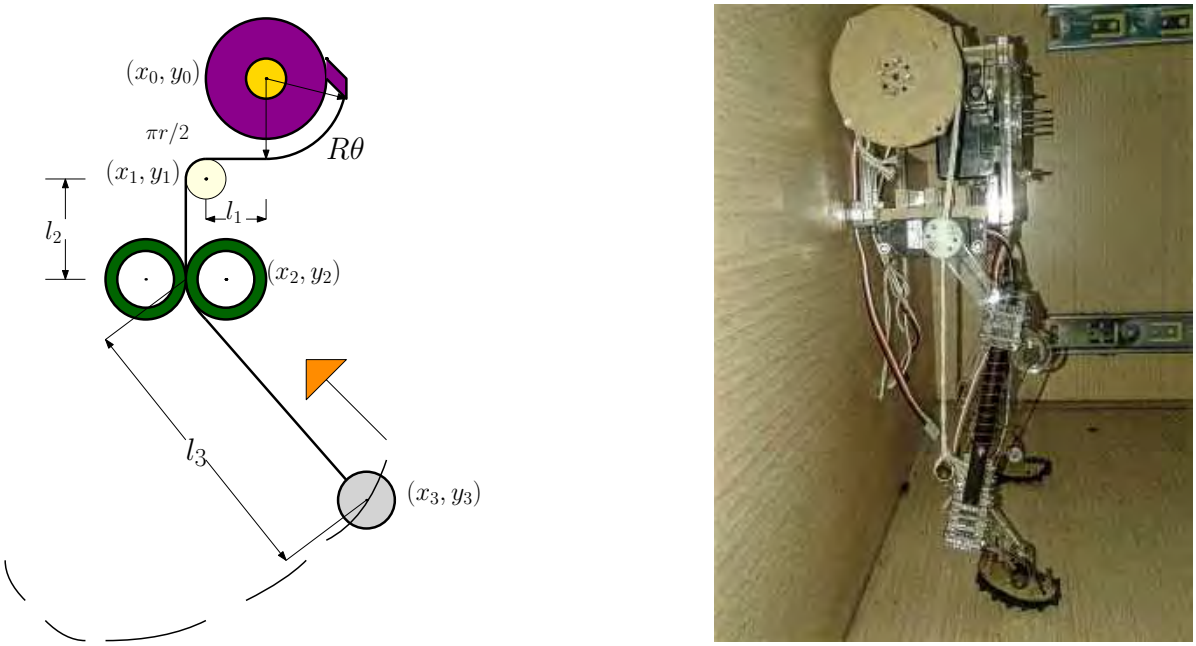

(a) (b)

Figure 4.2(a): Pulley mechanism for motion of the knee, Figure 4.2(b):Hardware model of individual module of prototype 2.

Flexible spine

The central part of our conjecture is the flexible spine. Our goal is not just to design and attend the flexibility but also leave room for modification on the hardware itself. For robots, changing stiffness at the nodes of the spine is hard compared to changing length and orientation of the rigid element. Keeping this idea in mind, we developed a flexible spine with different orientation of the elements.

For the rigid elements, we used laser machined Acrylic pieces. Same materials are also utilized in the development of the Gear-shaped component. The internal and external toothed components are cut from a single piece. This allows the teeth to have a tight lock once one is placed inside the other. The component has a resolution of 9 degrees per tooth rotation. These components enables us to provide the spine with any shape we desire without developing multiple components with various fixed orientations. For the flexible part, we have used thin polycarbonate strips, 6 mm, and secured them between two rigid elements. Use of polycarbonate strips is a suitable and is a more compact alternative for standard torsional springs. The picture of the actual spine utilized in the robot has been shown in fig. 4.2.

Tracked foot

The foot is an important aspect of the quadruped robot. It is also one of the most challenging aspects to design. As the slipping between the ground and the fast moving feet is a common phenomenon, it is

Figure 4.2: Physical model of the flexible spine

recommended to use high friction material at the bottom of the foot. After multiple trial and error, we have used tracks in the lower part of the foot to provide maximum traction. In fig. 4.3 we have shown the hardware model of the tracked foot.

Figure 4.3: Foot with tracked shoe

4.3 Simulation development and results

To test our hypothesis, we started developing a robot, Prototype 1, which is similar to cheetah-cub. Cheetah-cub[32] is a rigid body quadruped robot with compliant legs and string-driven knee joints. The success of the Prototype 1 allowed us to develop further and design more complicated model of the quadrupeds, i.e. Prototype 2.

4.3.1 CAD model

The first prototype was designed as the proof of concept of the quadruped robot. We used the make block servo motor as the primary attachment between the legs and the central structure. The modules hosting the servo motor are designed to be same for both front and hind part of the robot. All these features can be seen in the complete assembly of the robot in fig. 4.4(a). In ”Prototype 2” modules/multiple motor housings were created to accommodate the new servo motor. Details drawing of modules and the rigid spine can be found in Appendix B.

(a) CAD model of the quadruped robot, Prototype 3

(b) Simulation model designed in webots.

Figure 4.4: CAD model and simple geometry simulation model

Once we have developed a CAD model of the quadruped we go on to simulate it in *Webots*[33], a physics simulation software. This simulator allows us to make the designs as real as possible, minimizing the error encountered while developing a physical model.

4.3.2 Simulation

The primary purpose of the simulation is to conduct as many experiments as possible without reducing the life of the physical model or increasing the cost of the design. Also, simulation allows us to test various controllers that would other wise be very expensive to test on real robots. To simulate we have used **webots** as the simulation software. There we have made a model of a rigid quadruped robot to test our hypothesis. We used CPG as the primary controller for this simulation. We used the multi segmented spine, fig. 4.4(b), with very high nodal torsional stiffness at the hinges to make the robot behave as a rigid spine robot.

For a smooth simulation, we have used simple collision shapes while designing this robot in webots.

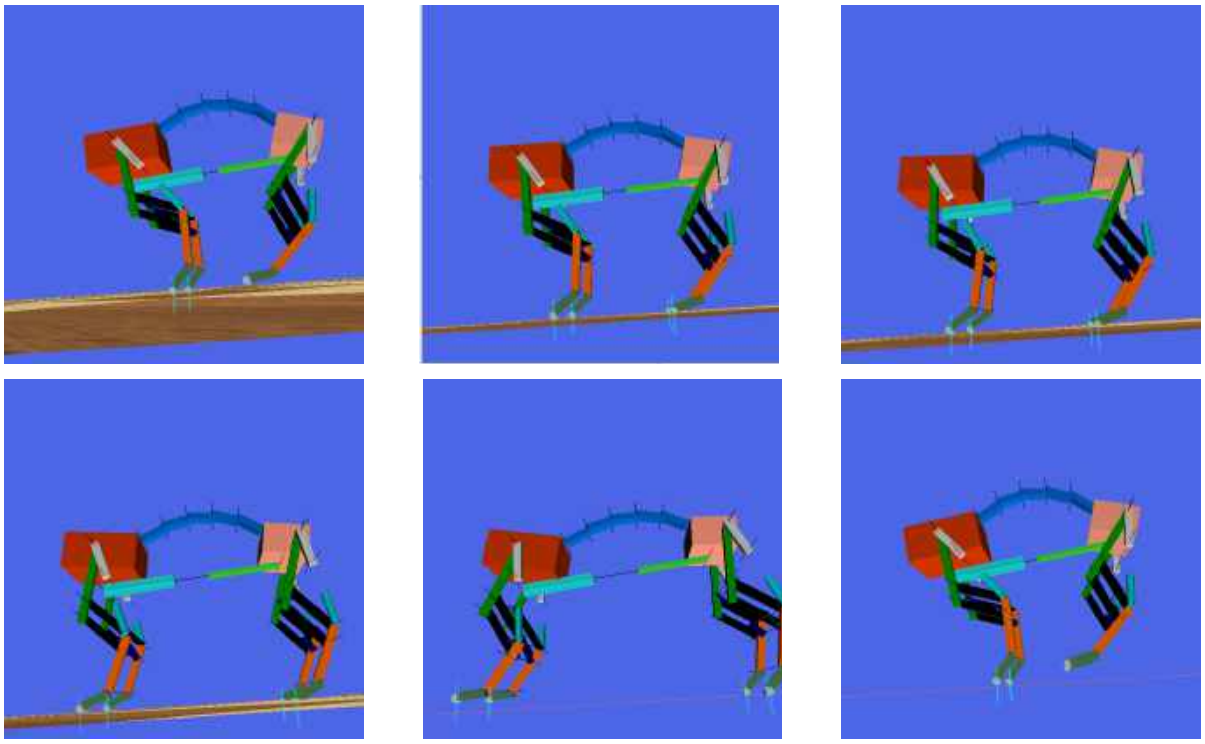

Figure 4.5: Simulation of a flexible spine quadruped on bounding gait

4.4 Control strategy

So far all the discussion was about the design, simulation of the quadruped robot. In this section, the control strategies involved with motion of the quadruped robots will be discussed in details. In everyday life, we mostly observe two types of locomotion around us. First being the discrete type locomotion and second being the rhythmic form of locomotion. Walking, running, scratching or any periodic motion falls under the category of rhythmic locomotion or movement. Since we are dealing with quadruped locomotion, specifically bounding gait, we will deal with rhythmic movement only. In this work, we consider the approach taken to design the controller of cheetah-cub, coupled nonlinear oscillators. In section 4.4.1 we describe how the oscillators work and how they can be combined to generate the desired gaits.

4.4.1 Controllers

We used central pattern generator (CPG) as the main controller for the robot. The idea of central pattern generator was introduced in biological science to explain the rhythmic behavior in the animal motion. In 1985, studies conducted by Matsuoka, K. [39] uses an artificial neural network to generate various patterns. However, ANN is computation intensive. To avoid significant computation and to generate

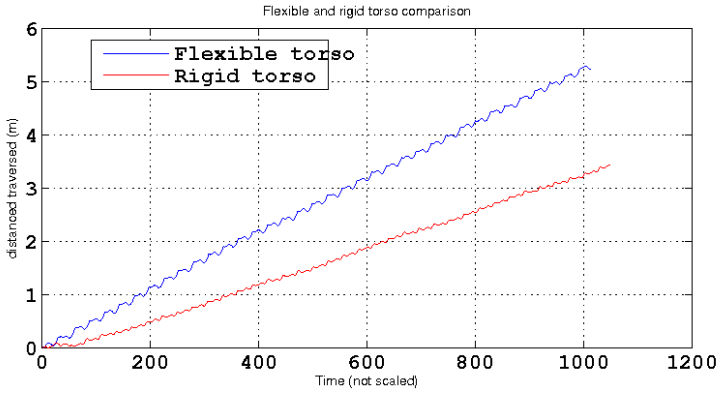

Figure 4.6: Distance covered by a flexible spine quadruped and a rigid spine quadruped via bounding gait

a simple parameterization, the nonlinear oscillator is a preferable choice for the pattern generator. To develop the controller we followed into the works of Auke Jan Ijspreet [40, 41, 42, 43] related to the use of nonlinear oscillator as CPG. In the works done by A.Sprowitz[32] and Eckert[6], a simplified CPG is used to control the motion of the quadruped. This open loop strategy is both self stabilizing and cost effective. In section 4.4.1 we describe the mathematical formulation of the CPG.

Abbri.		Abbri.	
ϕ_i	oscillator linear phase	$O^{[h,k]}$	Desired offset of hips/knees
f	Stride frequency	$A^{[h,k]}$	Amplitude of hips/knees
$k_{i,j}$	Coupling between hips	$o^{[h,k]}$	Instantaneous offset of hip/knee
$\varphi_{i,j}$	Phase difference between hips	$a^{[h,k]}$	Instantaneous amplitude of hip/knee
$\varphi_{h,k}$	Phase difference between hip and knee.	D_{vir}	Virtual duty factor
Γ_i^h	Hip motor input/ Hip joint angle	$\Theta_i^{[h,k]}$	Phase of hip/knee joint
Γ_i^k	Knee motor input	A_{st}	Amplitude in stance phase
α	Time constant	A_{sw}	Amplitude in swing phase

Table 4.1: Nomenclature of the terminologies used in CPG

Mathematical formulation

There are two parts of the non-linear oscillator based controller design. First, the coupled hip movement and second, the hip and knee coupling. Gaits, such as bound, gallop, trot, canter can be generated with the help of the coupling between the oscillators in the hips. By solving equation (4.1) to (4.5) we

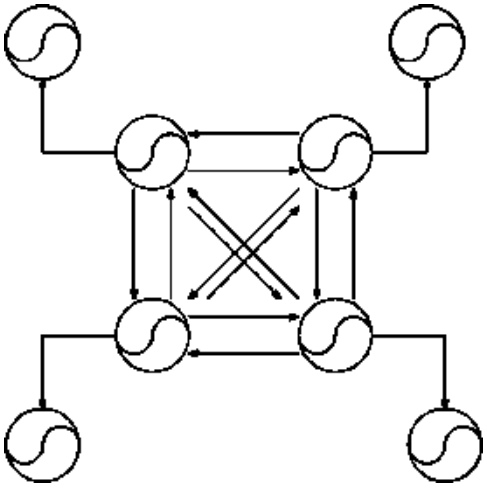

(a)

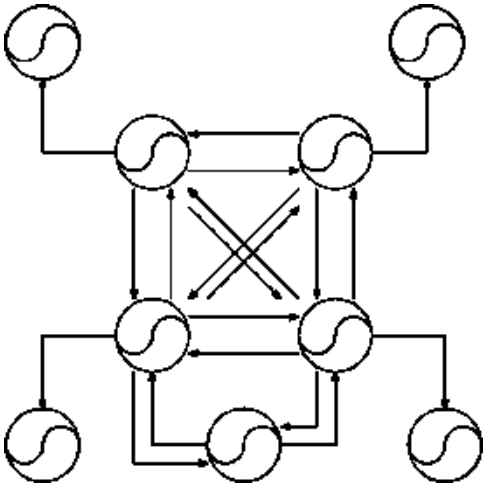

(b)

(c)

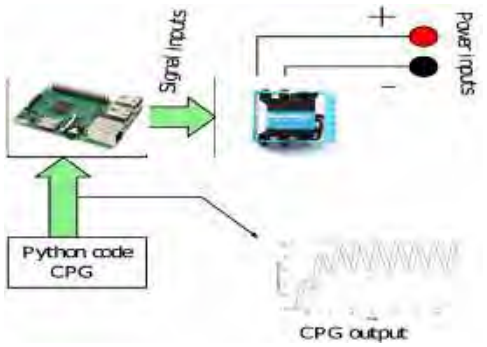

(d)

Figure 4.7(a): Central pattern generator for a quadruped robot with rigid spine, Figure 4.7(b): Central pattern generator for a quadruped robot with flexible spine, Figure 4.7(c) Raspberry pi 3b as the hardware for the controller, Figure 4.7(d) describes how the servos are controlled with help of CPG.

generate the movement pattern of the hips.

$$\dot{\phi}_i = 2\pi f + \sum_{j \neq i} k_{i,j} \sin(\phi_j - \phi_i - \varphi_{i,j}) \tag{4.1}$$

$$\dot{a}_i^h = \alpha(A_i^h - a_i^h) \tag{4.2}$$

$$\dot{o}_i^h = \alpha(O_i^h - o_i^h) \tag{4.3}$$

$$\Theta_i^h = \begin{cases} \dfrac{\phi_i}{2D_{vir}} & 0 \leq \phi_i \leq 2\pi D_{vir} \\ \dfrac{\phi_i + 2\pi(1 - 2D_{vir})}{2(1 - D_{vir})} & \end{cases} \tag{4.4}$$

$$\Gamma_i^h = a_i^h \cos\left(\Theta_i^h\right) + o_i^h \tag{4.5}$$

Once the coupled hip motion is solved, the solutions of the hips are sent their respective knee. The coupling between hip and knee motion creates the signal the drives the knee motor from the hip signal.

$$\Theta_i^k = \Theta_i^h + \varphi_{h,k} \tag{4.6}$$

$$a_i^k = \begin{cases} A_{st} & \Theta_i^k \leq \pi \\ A_{sw} & \Theta_i^k \geq \pi \end{cases} \tag{4.7}$$

$$\dot{o}_i^k = \alpha(O_i^k - o_i^k) \tag{4.8}$$

$$\theta = 2\left[\frac{\Theta_i^k}{2\pi} \mod (0.5)\right] \tag{4.9}$$

$$\gamma_i = \begin{cases} -16\theta^3 + 12\theta^2 \\ 16(\theta - 0.5)^3 - 12(\theta - 0.5)^2 + 1 \end{cases} \tag{4.10}$$

$$\Gamma_i^k = a_i^k \gamma_i + o_i^k \tag{4.11}$$

The signals sent to the servo motors are obtained by solving equation (4.5) and (4.11) respectively.

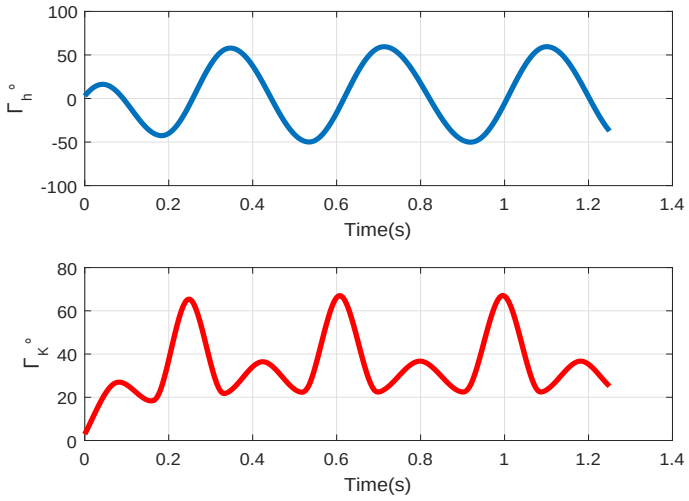

Figure 4.7: Outputs of the CPG sent to the servo motors

4.5 Prototype development and experiment

To test our hypothesis, we developed two robots, a rigid spine (Figure 4.9(a)) quadruped robot and a flexible spine quadruped robot(Figure 4.9(b)). In the simulation result, we have already seen the flexible spine quadruped robot performs better, which is to say running faster, than the rigid spine quadruped robot under the same bounding gait. In fig. 4.10, we display the movement of "Prototype

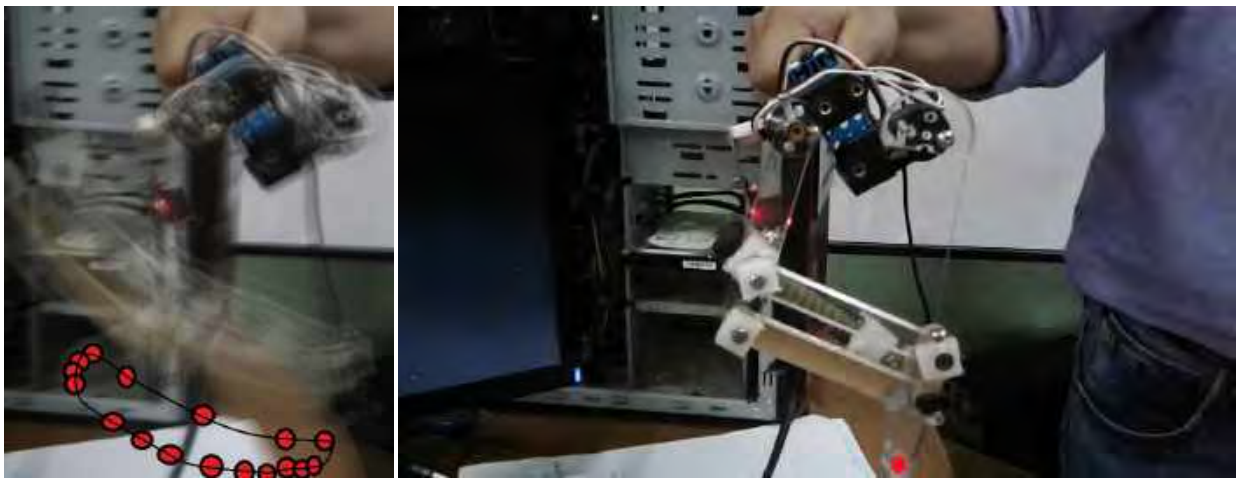

(a) Trajectory highlighted (b) Compliant leg, red dot represt the point being tracked

Figure 4.8: Trajectory generated by the complaint leg using CPG

Hardware	Function	Number
Makeblock servo (Prototype 1)	Actuator	8
Kondo KRS2350 servo (Prototype 2)	Actuator	9
Raspberry Pi 3b	Onboard computation	1
Compression spring	Compliance and energy storage	4x2
11.3V, 2200mah LiPo Battery pack (Prototype 2)	Power source for the motors	1
Standard power-bank (Prototype 2)	Power source for the raspberry pi	1
Torsion springs	Absorption of the impact load and stability of the foot	4
Polycarbonate strips (Prototype 2)	Generate flexibility in the spine	4
Fuse 1.25A	Servo over-current protection	9
VNC Viewer & Smart phone	Communication and display unit (USB)	1

Table 4.2: Components used to make the quadruped

1″ while executing a trot gait.

4.6 Observations made during experiment

- During the experiment the disparity between simulation and experiment became apparent. In the simulation, the slipping of the foot and ground were not a very important issue, as the contact model in the simulator has been simplified for a more real-time simulation. However, in the physical model, it is an important factor. To counter that we have used tracked shoes, which improved the friction between the foot and the ground.

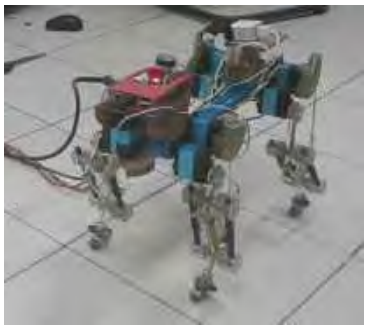

(a) Quadruped robot with rigid spine, Prototype 1

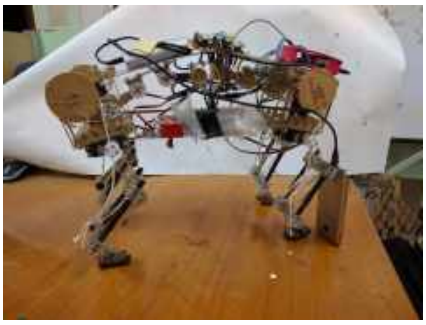

(b) Quadruped robot with flexible spine, Prototype 2.

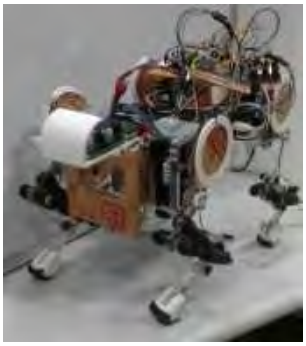

(c) Quadruped robot with rigid spine, Prototype 3

Figure 4.9: Robot developed for hardware testing.

(a) 1

(b) 2

(c) 3

(d) 4

(e) 5

(f) 6

Figure 4.10: Hardware testing of a rigid spine quadruped on trot gait

- The flexibility of the spine helps the robot move faster but at the cost of stability of the structure. This instability became noticeable with the second degree of freedom of the spine, Torsional motion.
- The height of center of mass and the width of the robot are also important for the stability. The height of the center of mass was high in Prototype 2. Along with a leaner design than Prototype 1, the robot became unstable to some extent.
- The torsion spring placed between foot and the leg was not soft enough to reduce the effect of impact on the robot.
- During the development, we used the structure of the servos as a part of the primary load bearing structure for prototype 1. For time being it seemed ok, but over time the motor casings began to

come off due to shock and vibration generated due to impact.

4.7 Summary

In this chapter, we discussed the design, control, simulation and experiment of the quadruped robots with both flexible and rigid spine. In the design section, we discussed on how the legs, foot, spine, and knee mechanism worked. In the control section, we discussed on how to create open-loop synchronous oscillators which can help the robot to walk. In simulation part, we discussed on how to create a model in webots and tested it.

Chapter 5

Conclusions

5.1 Summary

This thesis is an attempt to design flexible spine for a quadruped robot by using optimization. The main reasons for such a change is the ability of the scheme to provide the user with the control of the static and dynamics response property of the spine. In chapter 1, the motivation, literature survey and challenges associated with the designing of flexible spine are discussed. It is shown most of the quadrupeds developed have a rigid spine, only a few has flexible spine. The chapter ends with the scope and contribution of the thesis.

Chapter 2 presents idea of pseudo rigid body model and transformation between continuous beams to lumped model system.The flexible structure is modeled as a series of rigid segments with springs and dampers at the joints. It is shown there is an analytical relationship between the continuous beam and a pseudo rigid model, for small deflection. Additionally, the chapter also contains multiple example of comparison between FEM results and pseudo rigid modeling.

Chapter 3 discusses optimization scheme to develop the flexible spine. A parameter optimization based approach is used to develop a spine like structure with the constraints provided by both the user and the manufacturing process. The optimization problem has been solved for some standard forces generated by the human body. It is shown that when large number of links are used, the optimization scheme would prefer one set of variable over another. The results for 10 links shows unless the magnitudes are scaled the scheme prefers to change the shape over stiffness. Additionally, another gradient based optimization scheme has been used to obtain the user prescribed response time from the flexible structure. Finally, it is shown, the flexible spine obtained with the help of these optimization scheme, can respond to periodic loading of low frequency equally well.

Chapter 4 deals with the design, simulation, and hardware modeling of two quadruped robot. This

chapter also gives a detailed description of the CAD model, various mechanical aspect of the robot, the control strategy implemented using python and raspberry pi 3b. Multiple simulation runs and a few experimental runs were conducted in the laboratory. It is shown in the simulation model the flexible spine quadruped moves at a much higher speed than a rigid spine quadruped robot. It is also shown the problems associated with the design and development of the quadruped robot.

5.2 Scope of future works

The approach and the results reported in this work can be extended in several ways. We list some of the main ones below. In future models, we need to address this issues and build a more robust structure.

1. In spite of the simulation results showing the requirement of our hypothesis when implemented in hardware, it 's hard to establish the premises just yet.

2. Both the robots have flaws when it comes to impact. First, the system we designed is still too rigid for the absorption impulsive-load, resulting the body to experience high impulse every time it moves. Second, the closed pantograph style legs are also an issue. Open pantograph style legs with spring loading allow the system to be a much better shock absorber, a feature we overlooked. Third, the spine flexibility is itself an issue. We have already discussed the trade-off between flexibility and rigidity.

3. During the hardware experiments, we came across the torsional flexibility, due to nature of our spine. This relative motion caused undesired deflection in the structure during trot gait.

4. In terms of controller it is an open loop system. In future it can be extend it to closed loop system with camera, force sensor and IMU modules.

Appendix A

Expressions for gradients

In this Appendix, the details of the mathematics for the case of large deflection case are presented. The internal energy stored due to the passive loading is $\mathcal{J}$. This and the constraints, Φ_1 Φ_2, are given as

$$\mathcal{J} = \frac{1}{2}\Delta\theta_1^T \mathbf{K}_m \Delta\theta_1. \tag{A.1}$$

$$\Phi_1 = \sum_{i=1}^{N} L_i \sin\theta_{0,i} \tag{A.2}$$

$$\Phi_2 = \sum_{i=1}^{N} L_i \left(\cos\theta_{2,i} - \cos\theta_{0,i}\right) \tag{A.3}$$

where, θ_0 is the vector of initial undeformed angles, $\Delta\theta_1$ is the vectors of the angular deflection due to the passive loading $\mathcal{P}(\theta_1)$, θ_2 is the vectors of the final state of the angles due to the passive and active loading combined, $\mathcal{P}(\theta_2)$. Combining all the constraints and objective function we generate the Lagrangian. It is given by

$$\mathcal{L} = \mathcal{J} + \Lambda_1\Phi_1 + \Lambda_2\Phi_2 \tag{A.4}$$

where, $\Lambda_1,\ \Lambda_2$ are Lagrange multipliers. Now we compute the gradients of the Lagrangian with respect to the design variables ($K,\ \theta_0$). Here K is a $(N+1\times 1)$ vector, and θ_0 in a $(N\times 1)$ vector. $K_i,\ \theta_{0,i}$ are

the i^{th} element of the vectors. The gradient with respect to individual elements are as followed.

$$\begin{aligned}
\frac{d\mathcal{L}}{dK_i} &= \frac{d\mathcal{J}}{dK_i} + \Lambda_1 \frac{d\Phi_1}{dK_i} + \Lambda_2 \frac{d\Phi_2}{dK_i} && \text{(A.5)}\\
&= \frac{d\mathcal{J}}{dK_i} - \Lambda_2 \sum_{j=1}^{N} L_j \sin\theta_{2,j} \frac{d\theta_{2,j}}{dK_i} && \text{(A.6)}\\
&= \frac{1}{2}\Delta\theta_1^T \frac{d\mathbf{K}_m}{dK_i}\Delta\theta_1 + \Delta\theta_1^T \mathbf{K}_m \frac{d\theta_1}{dK_i} - \Lambda_2 \sum_{j=1}^{N} L_j \sin\theta_{2,j} \frac{d\theta_{2,j}}{dK_i}
\end{aligned}$$

$$\begin{aligned}
\frac{d\mathcal{L}}{d\theta_{0,i}} &= \frac{d\mathcal{J}}{d\theta_{0,i}} + \Lambda_1 \frac{d\Phi_1}{d\theta_{0,i}} + \Lambda_2 \frac{d\Phi_2}{d\theta_{0,i}}\\
&= \frac{d\mathcal{J}}{d\theta_{0,i}} + \Lambda_1 L_i \cos\theta_{0,i} - \Lambda_2 \sum_{j=1}^{N} L_j \sin\theta_{2,j} \frac{d\theta_{2,j}}{d\theta_{0,i}} + \Lambda_2 L_i \sin\theta_{0,i} && \text{(A.7)}\\
&= \Delta\theta_1^T \mathbf{K}_m \left[\frac{d\theta_1}{d\theta_{0,i}} - \frac{d\theta_0}{d\theta_{0,i}}\right] + \Lambda_1 L_i \cos\theta_{0,i} - \Lambda_2 \sum_{j=1}^{N} L_j \sin\theta_{2,j} \frac{d\theta_{2,j}}{d\theta_{0,i}} + \Lambda_2 L_i \sin\theta_{0,i} && \text{(A.8)}
\end{aligned}$$

$$\begin{aligned}
\begin{pmatrix} \frac{d\theta_2}{dK_i} \\ \frac{d\lambda}{dK_i} \end{pmatrix} &= \begin{bmatrix} \mathbf{K}_m - \nabla_{\theta_2}\mathcal{P}(\theta_2) & -\frac{d\mathcal{P}(\theta_2)}{d\lambda} \\ \nabla_{\theta_2}\Phi_3^T & 0 \end{bmatrix}^{-1} \begin{pmatrix} -\frac{d\mathbf{K}_m}{dK_i}\Delta\theta_2 \\ 0 \end{pmatrix} && \text{(A.9)}\\
\begin{pmatrix} \frac{d\theta_2}{d\theta_{0,i}} \\ \frac{d\lambda}{d\theta_{0,i}} \end{pmatrix} &= \begin{bmatrix} \mathbf{K}_m - \frac{d\mathcal{P}(\theta_2)}{d\theta_2} & -\frac{d\mathcal{P}(\theta_2)}{d\lambda} \\ \nabla_{\theta_2}\Phi_3^T & 0 \end{bmatrix}^{-1} \begin{pmatrix} \mathbf{K}_m \frac{d\theta_0}{d\theta_{0,i}} \\ 0 \end{pmatrix}.
\end{aligned}$$

where, $\mathbf{K}_m$ is the stiffness matrix used in equilibrium equation. The form of $\mathbf{K}_m$ is given as follows:

$$\mathbf{K}_m = \begin{bmatrix}
K_1 + K_2 & -K_2 & . & . & 0 & 0 \\
-K_2 & K_2 + K_3 & -K_3 & . & . & 0 \\
. & . & . & . & . & . \\
. & . & -K_i & K_i + K_{i+1} & -K_{i+1} & . \\
. & . & . & . & . & . \\
0 & . & . & -K_{N-1} & K_{N-1} + K_N & -K_N \\
0 & 0 & . & . & -K_N & K_N + K_{N+1}
\end{bmatrix} \qquad \text{(A.10)}$$

here, λ represents the Lagrange multiplier introduced for the constraint, equation (A.11), to generate the equilibrium equations. The Λ_i and λ are of generated from two different optimization problems.

The constraint for the large deflection, Φ_3,

$$\Phi_3 = \sum_{i=1}^{N} L_i \sin\theta_i.$$

$$\nabla_\theta \Phi_3 = \begin{pmatrix} . \\ . \\ . \\ L_j \cos\theta_j \\ . \\ . \\ . \end{pmatrix}$$

P_X and P_Y are vectors containing the forces applied at the nodes along X-axis and Y-axis. For the problem discussed, other than $P_{X,N+1}$ all other $P_{X,i}$ are zeros. The load vector for the equilibrium equation for large deflection is as followed.

$$\begin{aligned}
\mathcal{P}(\theta) &= \mathcal{L}_\mathcal{C}\mathcal{A}P_Y - \mathcal{L}_\mathcal{S}\mathcal{A}P_X + \lambda\nabla_\theta\Phi_3; && \text{(A.11)}\\
\frac{d\mathcal{P}}{d\theta_i} &= \frac{d\mathcal{L}_\mathcal{C}}{d\theta_i}\mathcal{A}P_Y - \frac{d\mathcal{L}_\mathcal{S}}{d\theta_i}\mathcal{A}P_X + \lambda\frac{d\nabla_\theta\Phi_3}{d\theta_i};\\
&= \frac{d\mathcal{L}_\mathcal{C}}{d\theta_i}\begin{bmatrix} . \\ . \\ \sum_{j=k}^{N+1} P_{Y,j} \\ . \\ . \end{bmatrix} - \frac{d\mathcal{L}_\mathcal{S}}{d\theta_i}\begin{bmatrix} . \\ . \\ \sum_{j=k}^{N+1} P_{X,j} \\ . \\ . \end{bmatrix} - \lambda\begin{pmatrix} 0 \\ . \\ L_i\sin\theta_i \\ . \\ 0 \end{pmatrix};\\
&= -\begin{bmatrix} 0 \\ . \\ . \\ \sum_{j=i}^{N+1}\left(P_{Y,j}L_i\sin\theta_i + L_i\cos\theta_i P_{X,j}\right) + \lambda L_i\sin\theta_i \\ . \\ . \\ 0 \end{bmatrix} && \text{(A.12)}\\
\frac{d\mathcal{P}}{d\lambda} &= \nabla_\theta\Phi_3. && \text{(A.13)}
\end{aligned}$$

where,

$$\mathcal{L}_{\mathcal{C}} = \begin{bmatrix} L_1\cos\theta_1 & 0 & . & . & 0 & 0 \\ 0 & L_2\cos\theta_2 & 0 & . & . & 0 \\ . & 0 & L_3\cos\theta_3 & 0 & . & . \\ . & . & 0 & L_i\cos\theta_i & 0 & . \\ 0 & . & . & 0 & L_{N-1}\cos\theta_{N-1} & 0 \\ 0 & 0 & . & . & 0 & L_N\cos\theta_N \end{bmatrix} \tag{A.14}$$

$$\mathcal{L}_{\mathcal{S}} = \begin{bmatrix} L_1\sin\theta_1 & 0 & . & . & 0 & 0 \\ 0 & L_2\sin\theta_2 & 0 & . & . & 0 \\ . & 0 & L_3\sin\theta_3 & 0 & . & . \\ . & . & 0 & L_i\sin\theta_i & 0 & . \\ 0 & . & . & 0 & L_{N-1}\sin\theta_{N-1} & 0 \\ 0 & 0 & . & . & 0 & L_N\sin\theta_N \end{bmatrix} \tag{A.15}$$

$$\mathcal{A} = \begin{bmatrix} 1 & 1 & . & . & 1 & 1 \\ 0 & 1 & 1 & . & . & 1 \\ 0 & 0 & 1 & . & . & 1 \\ . & . & . & . & . & . \\ 0 & . & . & 0 & 1 & 1 \\ 0 & 0 & . & . & 0 & 1 \end{bmatrix} \tag{A.16}$$

Appendix B

Stages in quadruped development

In this chapter we will discuss various parts of the hardware design which are not directly relevant to the theory presented but essential towards the development of quadruped.

B.1 Detailed model of prototype 1

The ”Prototype 1” contained a string driven mechanism just like the Prototype 2. But the string do not pass through the node at the hip. This caused a loss of motion during the movement which is undesirable. The legs are provided with a two parallel compression spring rather than a single one to counter the bending moment developed due to the single spring. This feature was included in ”Prototype 2” for better and friction lock free leg design.

B.2 Detailed model of prototype 2

The ”Prototype 2” is developed by considering it to be a flexible spine quadruped. We previously showed the flexible spine model, made out of acrylic and polycarbonate material. Now we will describe the details of the model.

Development of the flexible spine started with the design of the rigid segment. In fig. B.2, a CAD model of a rigid segment is shown. Individual rigid link consists of four parts, the rigid central link (Red), the external toothed circle(Grey), a cover(White) and the internal toothed polycarbonate connector(Blue or the transparent component). The wide top on the connector(Blue) provides the mounting point for the polycarbonate strip. By varying the length of the polycarbonate strip, the nodal stiffness is designed.

The toothed components changes the angle between two rigid links to vary up to a certain extent. This allows us to change the shape of the spine, hence the overall stiffness. For all practical purposes,

Figure B.1: Pulley mechanism to drive knee motion for Prototype 1

changing the overall stiffness by rotating the toothed component is much cheaper than changing the flexible component while maintaining the same shape.

Modules

The design of the Prototype 2 required a new set of parts to house the Kondo motors. In **??** we describe the servo housing of the quadruped robot. Each servo housing/ module can contain up to 5 Servo motors. The pulley at the front of the housing is designed to mount the motor, moving the spine. On each side, two servo motors can be mounted to move the legs. Also the modules can house a host sensors and structures on the top and bottom of the servos.

The module is made out of acrylic material. By laser machining , components were produced in large numbers. The components are designed to be assembled by press fitting. This reduces the requirement of screws and unnecessary drills in the component.

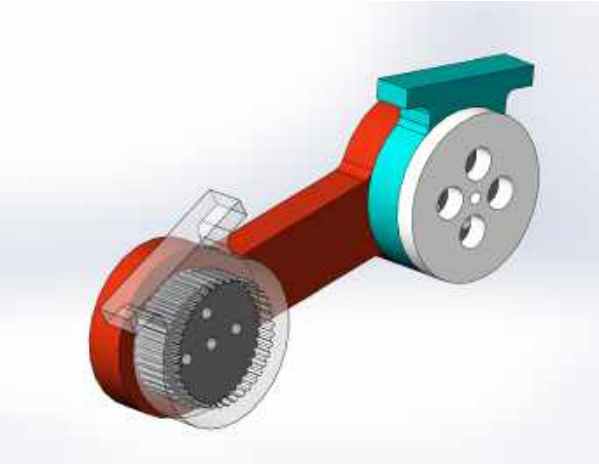

Figure B.2: Assembly model for the rigid segment

B.3 Details of prototype 3

The final prototype was designed with all the errors of ″Prototype 1″ and ″Prototype 2″ in mind. The robot was a rigid spine quadruped robot. In the following sections we introduce the design of quadruped robot.

The main body was made modular as ″Prototype 2″ and the modules can contain up to five servos each. Steel wire,(2mm) was used instead of nylon and cotton threads. The compliant segments were made more compact.

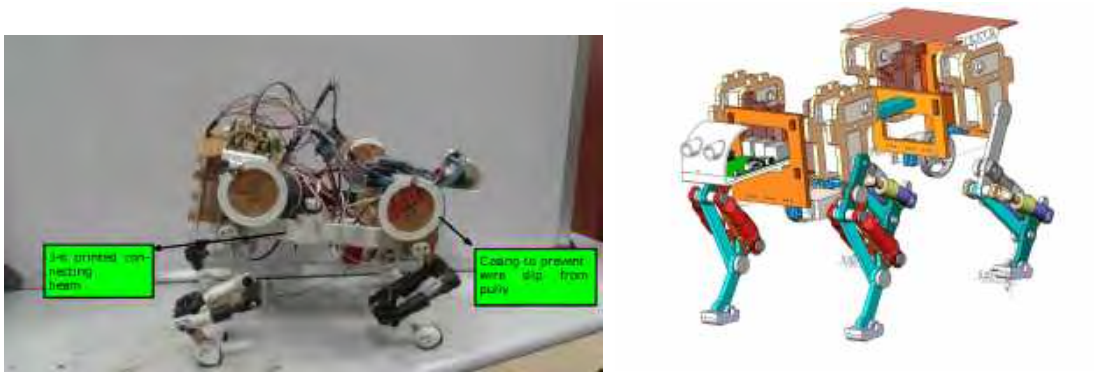

(a) Prototype 3 (b) CAD model of Prototype 3

Figure B.3

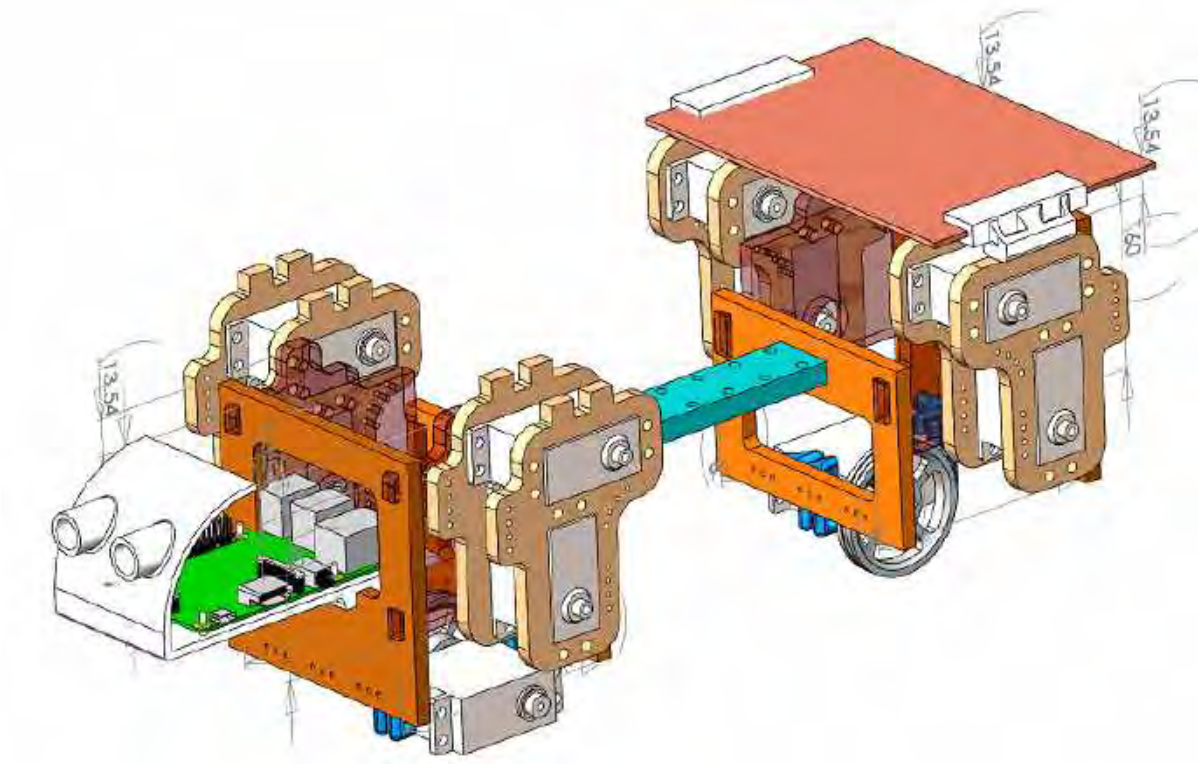

Figure B.4: Assembly of the body

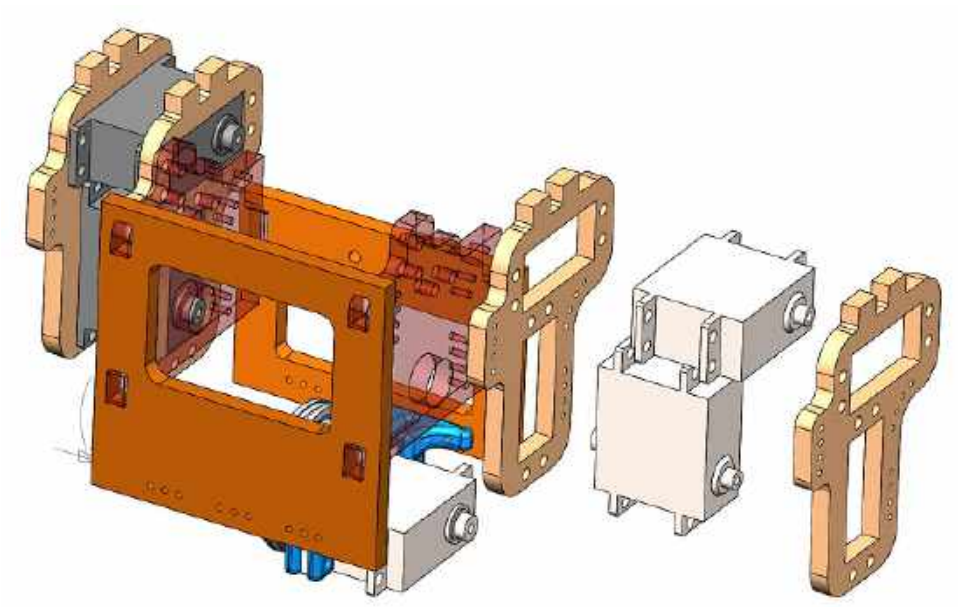

Figure B.5: Module and motor housing

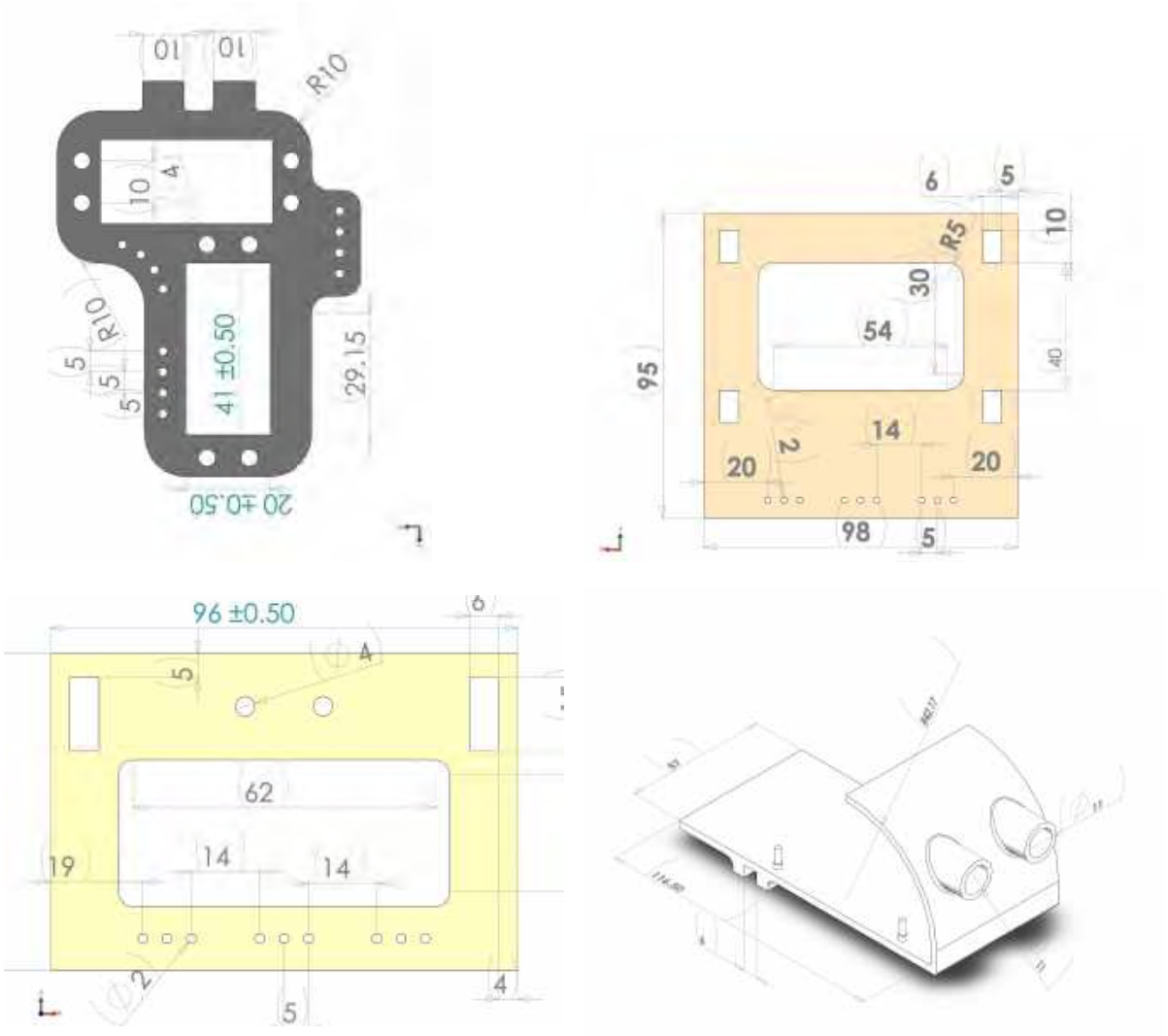

Figure B.6: Parts of the module

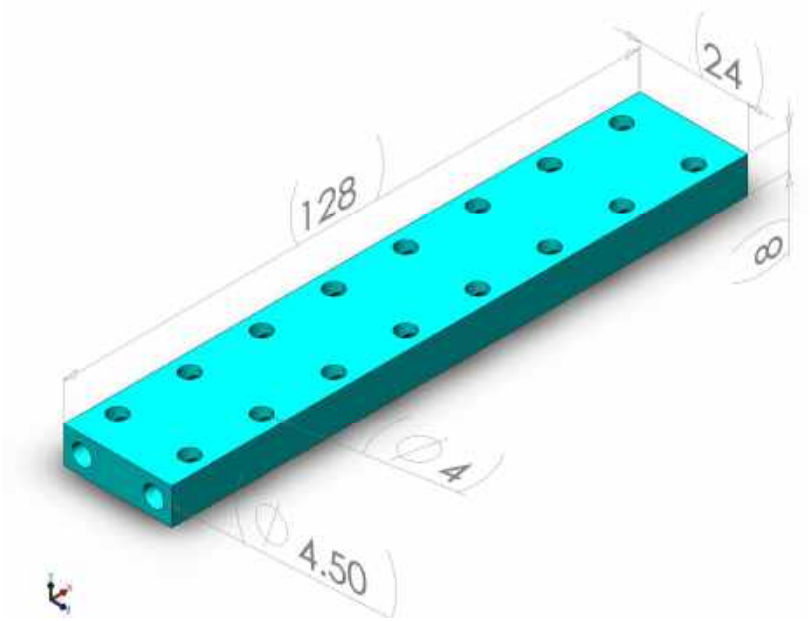

Figure B.7: Makeblock aluminum block

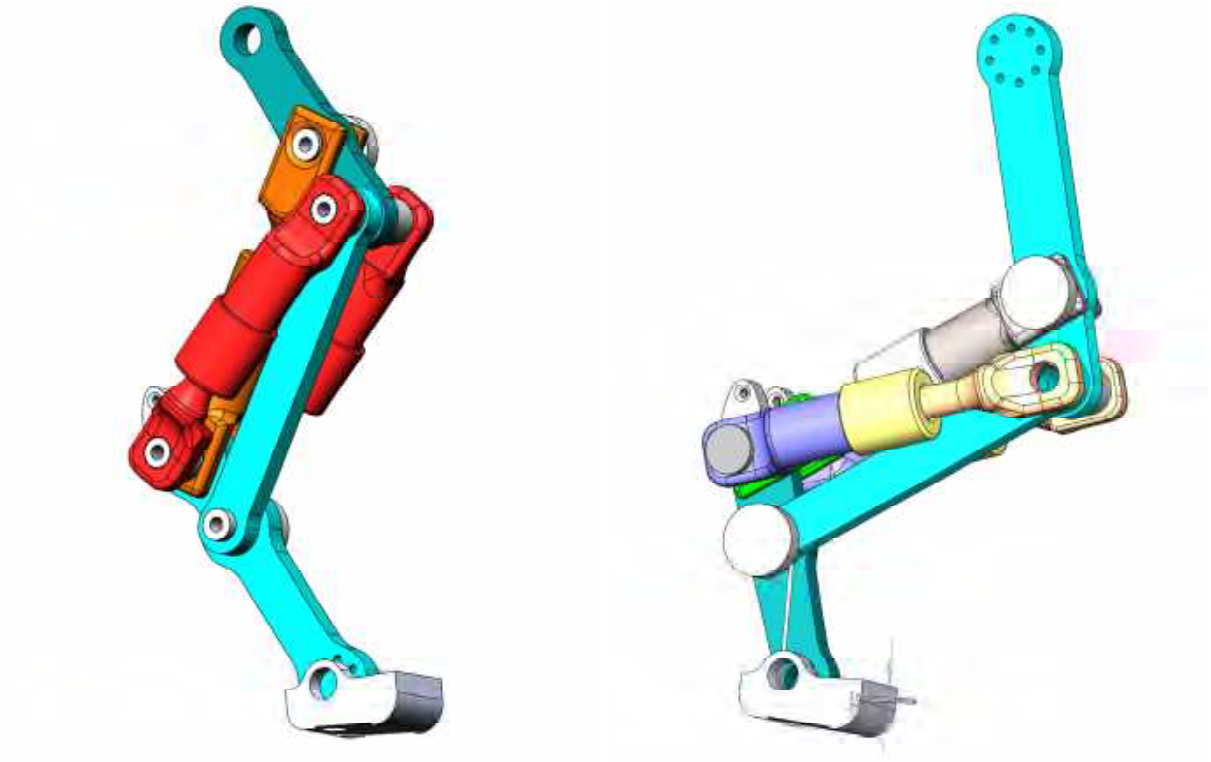

(a) Front leg

(b) Hind leg

Figure B.8

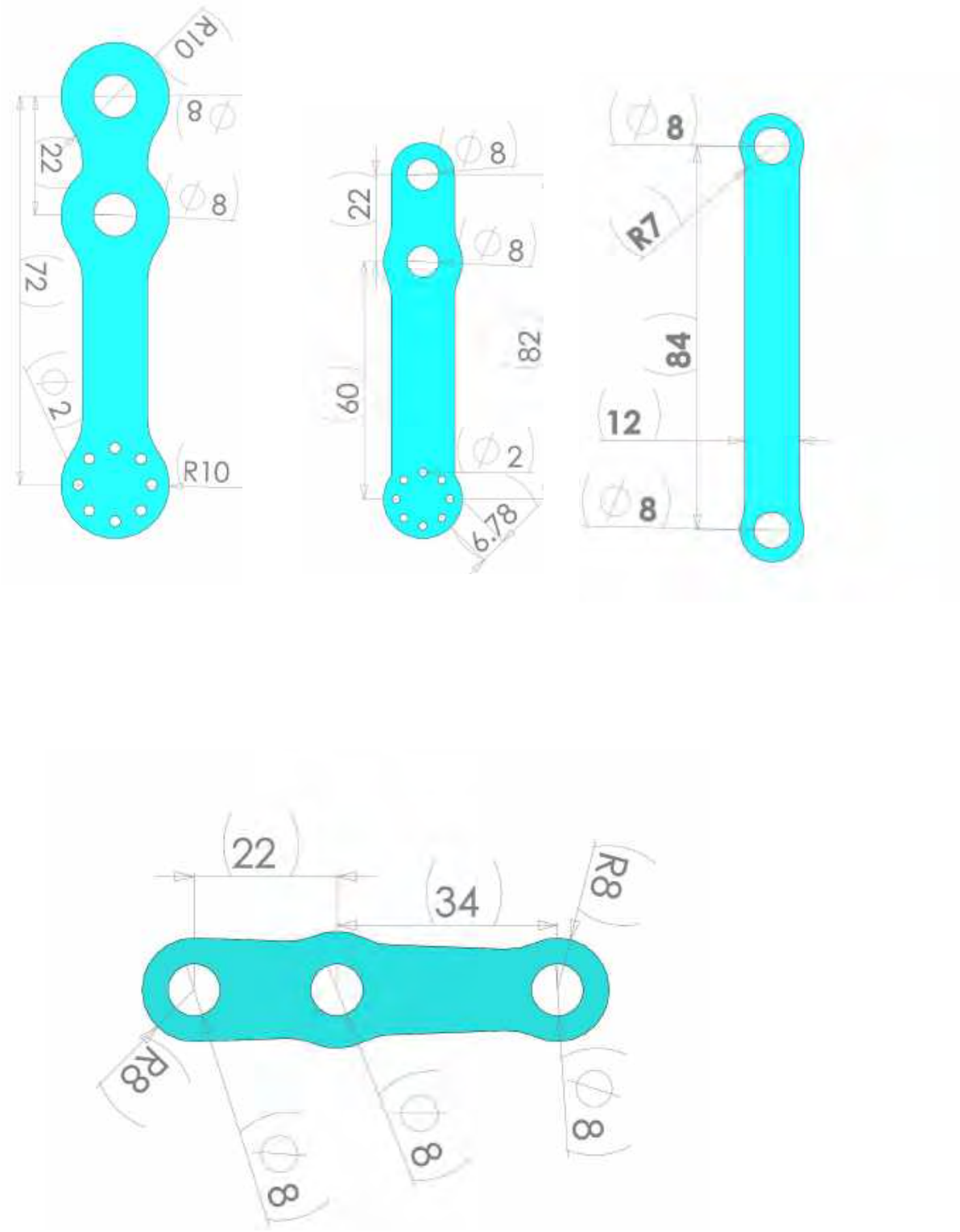

Figure B.9: Rigid links of the legs

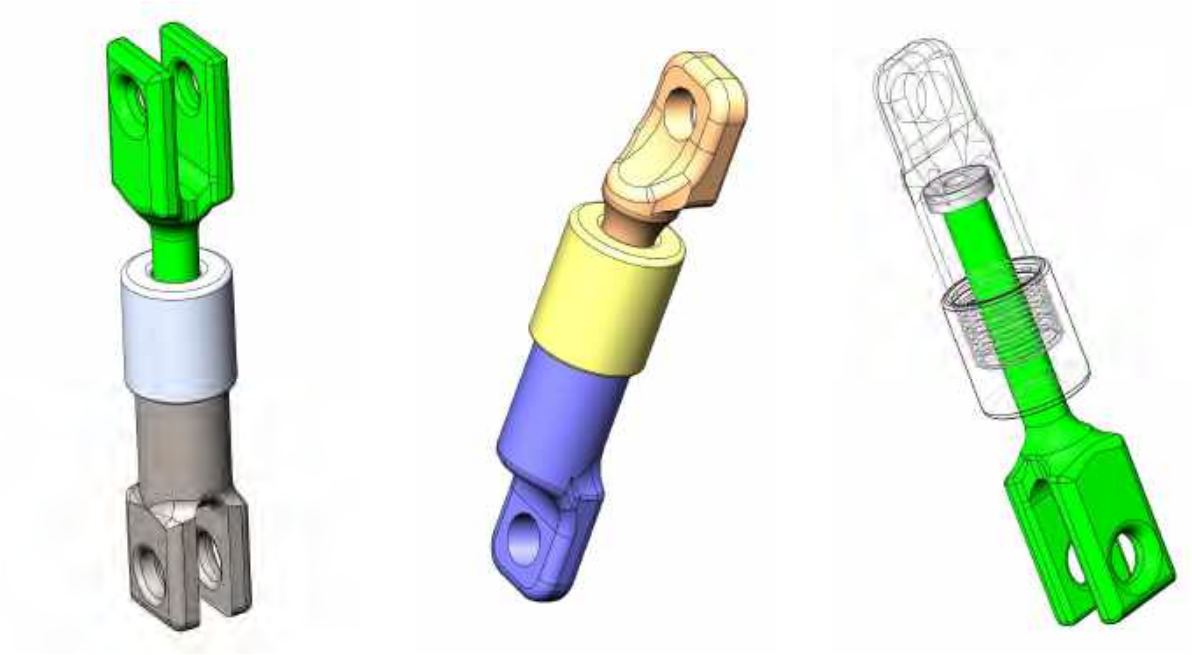

Figure B.10: Spring

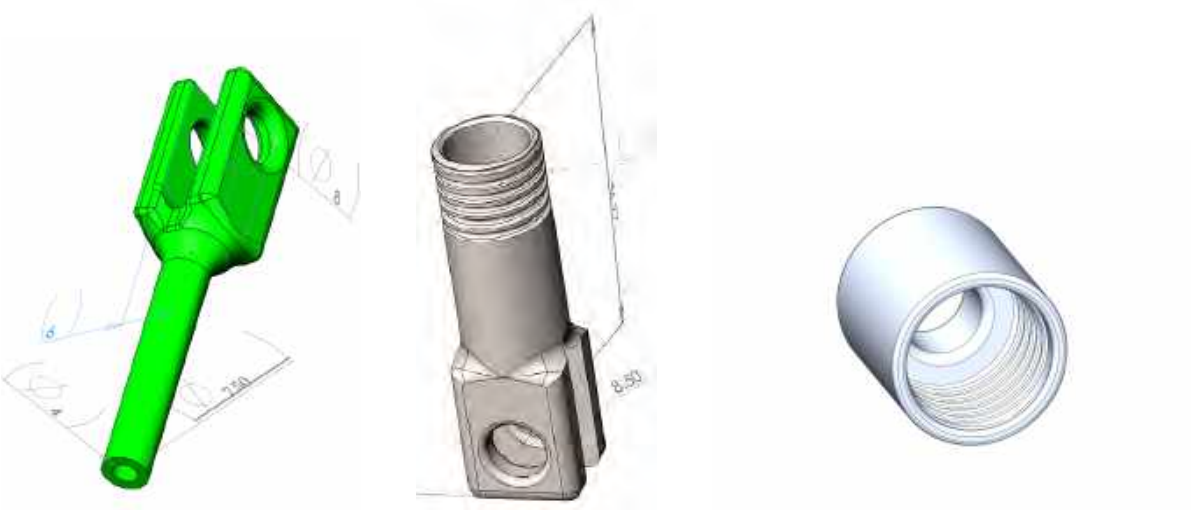

Figure B.11: Design for the springs

Appendix C

Derivation of the polynomial equation

By referring to the fig. 2.1, we can write

$$\delta = \sum_{i=1}^{n} L_i \theta_i$$

where δ is the deflection of the end point of the cantilever beam for equal L and K

$$\begin{aligned} \delta &= L\sum_{i=1}^{n} \theta_i \\ or,\ \delta &= L\sum_{i=1}^{n} i(\theta_i - \theta_{i+1}) \\ or,\ \alpha n^2 &= \sum_{i=1}^{n} i^2, \\ or,\ \frac{n^3}{3} + (\frac{1}{2} - \alpha)n^2 + \frac{n}{6} &= 0 \\ \theta_{n+1} &= 0 \end{aligned} \tag{C.1}$$

Where, $\alpha = \frac{K\delta}{Pn^2L^2}$

As a special case if γ is chosen as 1 we get

$$\frac{PL^2}{K}(\sum_{i=1}^{n} i^2 + (\gamma - 1)n^2) = \delta$$

which simplifies to

$$\frac{n^3}{3} + (\frac{1}{2} - \alpha)n^2 + \frac{n}{6} = 0$$

References

[1] Semini C., Tsagarakis N.G., Guglielmino E., Focchi M., Cannella F., and Caldwell D.G. Design of hyq–a hydraulically and electrically actuated quadruped robot. *Proceedings of the Institution of Mechanical Engineers, Part I: Journal of Systems and Control Engineering*, 2011.

[2] Hutter M.O., Gehring C., Jud D., Lauber A., Bellicoso C. D., Tsounis V., Hwangbo J., Bodie K., Fankhauser P., Diethelm B.R., et al. Anymal-a highly mobile and dynamic quadrupedal robot, 2016.

[3] Raibert M., Blankespoor K., Nelson G., Playter R., and Team T.B. Bigdog, the rough-terrain quadruped robot. In *Proceedings of the 17th World Congress*, volume 17, pages 10822–10825. Proceedings Seoul, Korea, 2008.

[4] Sprowitz A., Badri E., Khoramshahi M., Tuleu A., and Ijspeert A. Use your spine! effect of active spine movements on horizontal impulse and cost of transport in a bounding, quadruped robot. In *Proceedings of DW 2013*, number EPFL-CONF-186357, 2013.

[5] Seok S., Wang A., Chuah M.Y., Otten D., Lang J., and Kim S. Design principles for highly efficient quadrupeds and implementation on the mit cheetah robot. In *Robotics and Automation (ICRA), 2013 IEEE International Conference on*, pages 3307–3312. IEEE, 2013.

[6] Peter Eckert, Alexander Spröwitz, Hartmut Witte, and Auke Jan Ijspeert. Comparing the effect of different spine and leg designs for a small bounding quadruped robot. In *Robotics and Automation (ICRA), 2015 IEEE International Conference on*, pages 3128–3133. IEEE, 2015.

[7] Khoramshahi M., Sprowitz A., Tuleu A., Ahmadabadi M.N., and Ijspeert A. Benefits of an active spine supported bounding locomotion with a small compliant quadruped robot. In *Proceedings of 2013 IEEE International Conference on Robotics and Automation*, number EPFL-CONF-186299, 2013.

[8] Culha U. *An actuated flexible spinal mechanism for a bounding quadrupedal robot*. PhD thesis, Bilkent University, 2012.

[9] Cao Q. and Poulakakis L. Passive stability and control of quadrupedal bounding with a flexible torso. In *2013 IEEE/RSJ International Conference on Intelligent Robots and Systems*, pages 6037–6043. IEEE, 2013.

[10] Khoramshahi M., Bidgoly H.J., Shafiee S., Asaei A., Ijspeert A.J., and Ahmadabadi M.N. Piecewise linear spine for speed–energy efficiency trade-off in quadruped robots. *Robotics and Autonomous Systems*, 61(12):1350–1359, 2013.

[11] Lei J., Yu H., and Wang T. Dynamic bending of bionic flexible body driven by pneumatic artificial muscles (pams) for spinning gait of quadruped robot. *Chinese Journal of Mechanical Engineering*, 29(1):11–20, 2016.

[12] Haftka R.T. and Gürdal Z. *Elements of structural optimization*, volume 11. Springer Science & Business Media, 2012.

[13] Xu D. and Ananthasuresh G.K. Freeform skeletal shape optimization of compliant mechanisms. *Journal of Mechanical Design*, 125(2):253–261, 2003.

[14] Zhou H. and Ting K.L. Geometric modeling and optimization of multimaterial compliant mechanisms using multilayer wide curves. *Journal of Mechanical Design*, 130(6):062303, 2008.

[15] Howell L.L., Midha A., and Norton T.W. Evaluation of equivalent spring stiffness for use in a pseudo-rigid-body model of large-deflection compliant mechanisms. *Journal of Mechanical Design*, 118(1):126–131, 1996.

[16] Hai-Jun Su. A pseudorigid-body 3r model for determining large deflection of cantilever beams subject to tip loads. *Journal of Mechanisms and Robotics*, 1(2):021008, 2009.

[17] Chirikjian G.S. and Burdick J.W. A hyper-redundant manipulator. *IEEE Robotics and Automation Magazine*, 1(4):22–29, 1994.

[18] Conkur E.S. and Buckingham R. Clarifying the definition of redundancy as used in robotics. *Robotica*, 15(05):583–586, 1997.

[19] Ghosal A. *Robotics: fundamental concepts and analysis*. Oxford University Press, 2006.

[20] Seifried R. *Dynamics of underactuated multibody systems*. Springer, 2014.

[21] Alexander R.M.N. Why mammals gallop. *American zoologist*, 28(1):237–245, 1988.

[22] Hildebrand M. Motions of the running cheetah and horse. *Journal of Mammalogy*, 40(4):481–495, 1959.

[23] Hildebrand M. Further studies on locomotion of the cheetah. *Journal of Mammalogy*, 42(1):84–91, 1961.

[24] Ijspeert A.J., Crespi A., Ryczko D., and Cabelguen J.M. From swimming to walking with a salamander robot driven by a spinal cord model. *Science*, 315(5817):1416–1420, 2007.

[25] Roos L., Guenter F., Guignard A., and Billard A.G. Design of a biomimetic spine for the humanoid robot robota. In *The First IEEE/RAS-EMBS International Conference on Biomedical Robotics and Biomechatronics, 2006. BioRob 2006.*, pages 329–334. IEEE, 2006.

[26] Christophy M., Curtin M., Senan N.A.F., Lotz J.C., and OReilly O.M. On the modeling of the intervertebral joint in multibody models for the spine. *Multibody System Dynamics*, 30(4):413–432, 2013.

[27] MATLAB. Natick, massachusetts,, 2012.

[28] Lavaste F., Skalli W., Robin S., Roy-Camille R., and Mazel C. Three-dimensional geometrical and mechanical modelling of the lumbar spine. *Journal of Biomechanics*, 25(10):1153–1164, 1992.

[29] Sanchis-Moysi J., Idoate F., Dorado C., Alayón S., and Calbet J.A.L. Large asymmetric hypertrophy of rectus abdominis muscle in professional tennis players. *PLoS One*, 5(12):e15858, 2010.

[30] Akagi R., Takai Y., Ohta M., Kanehisa H., Kawakami Y., and Fukunaga T. Muscle volume compared to cross-sectional area is more appropriate for evaluating muscle strength in young and elderly individuals. *Age and ageing*, 38(5):564–569, 2009.

[31] Deb K. An introduction to genetic algorithms. *Sadhana*, 24(4-5):293–315, 1999.

[32] Alexander Spröwitz, Alexandre Tuleu, Massimo Vespignani, Mostafa Ajallooeian, Emilie Badri, and Auke Jan Ijspeert. Towards dynamic trot gait locomotion: Design, control, and experiments with cheetah-cub, a compliant quadruped robot. *The International Journal of Robotics Research*, 32(8):932–950, 2013.

[33] Olivier Michel. Cyberbotics ltd. webots: professional mobile robot simulation. *International Journal of Advanced Robotic Systems*, 1(1):5, 2004.

[34] Seok S., Wang A., Chuah M.Y. (Michael), Hyun D.J., Lee J., Otten D.M., Lang J.H., and Kim S. Design principles for energy-efficient legged locomotion and implementation on the mit cheetah robot. *IEEE/ASME Transactions on Mechatronics*, 20(3):1117–1129, 2015.

[35] Folkertsma G.A., Kim S., and Stramigioli S. Parallel stiffness in a bounding quadruped with flexible spine. In *2012 IEEE/RSJ International Conference on Intelligent Robots and Systems*, pages 2210–2215. IEEE, 2012.

[36] Kani M.H.H., Derafshian M., Bidgoly H.J., and Ahmadabadi M.N. Effect of flexible spine on stability of a passive quadruped robot: Experimental results. In *Robotics and Biomimetics (ROBIO), 2011 IEEE International Conference on*, pages 2793–2798. IEEE, 2011.

[37] Hong Zhou and Kwun-Lon Ting. Wide curve based geometric optimization of compliant mechanisms. In *Proceedings of the ASME Design Engineering Technical Conference, ASME*, 2005.

[38] Olivier A. Bauchau. *Flexible multibody dynamics*, volume 176. Springer Science & Business Media, 2010.

[39] Kiyotoshi Matsuoka. Sustained oscillations generated by mutually inhibiting neurons with adaptation. *Biological cybernetics*, 52(6):367–376, 1985.

[40] Auke Jan Ijspeert. A connectionist central pattern generator for the aquatic and terrestrial gaits of a simulated salamander. *Biological cybernetics*, 84(5):331–348, 2001.

[41] Alessandro Crespi, Daisy Lachat, Ariane Pasquier, and Auke Jan Ijspeert. Controlling swimming and crawling in a fish robot using a central pattern generator. *Autonomous Robots*, 25(1-2):3–13, 2008.

[42] Auke Jan Ijspeert. Central pattern generators for locomotion control in animals and robots: a review. *Neural networks*, 21(4):642–653, 2008.

[43] Simon Rutishauser, Alexander Sprowitz, Ludovic Righetti, and Auke Jan Ijspeert. Passive compliant quadruped robot using central pattern generators for locomotion control. In *Biomedical Robotics and Biomechatronics, 2008. BioRob 2008. 2nd IEEE RAS & EMBS International Conference on*, pages 710–715. IEEE, 2008.

[44] Bertram J. and Gutmann A. Motions of the running horse and cheetah revisited: fundamental mechanics of the transverse and rotary gallop. *Journal of the Royal Society Interface*, pages rsif–2008, 2008.

[45] Boyd S. and Vandenberghe L. *Convex optimization*. Cambridge University press, 2004.

[46] Cao Q. and Poulakakis L. Quadrupedal bounding with a segmented flexible torso: passive stability and feedback control. *Bioinspiration & biomimetics*, 8(4):046007, 2013.

[47] Chen D., Liu Q., Dong L., Wang H., and Zhang Q. Effect of spine motion on mobility in quadruped running. *Chinese Journal of Mechanical Engineering*, 27(6):1150–1156, 2014.

[48] Chirikjian G.S. and Burdick J.W. An obstacle avoidance algorithm for hyper-redundant manipulators. In *Robotics and Automation, 1990. Proceedings., 1990 IEEE International Conference on*, pages 625–631. IEEE, 1990.

[49] Chirikjian G.S. and Burdick J. W. A modal approach to hyper-redundant manipulator kinematics. *IEEE Transactions on Robotics and Automation*, 10(3):343–354, 1994.

[50] Culha U. and Saranli U. Quadrupedal bounding with an actuated spinal joint. In *Robotics and Automation (ICRA), 2011 IEEE International Conference on*, pages 1392–1397. IEEE, 2011.

[51] Deng Q., Wang S., Xu W.and Mo J., and Liang Q. Quasi passive bounding of a quadruped model with articulated spine. *Mechanism and Machine Theory*, 52:232–242, 2012.

[52] Goto M., Kawai M., Nakata M., Itamoto K., Miyata H., Ikebe Y., Tajima T., and Wada N. Distribution of muscle fibers in skeletal muscles of the cheetah (acinonyx jubatus). *Mammalian Biology-Zeitschrift für Säugetierkunde*, 78(2):127–133, 2013.

[53] McMahon T.A. and Cheng G.C. The mechanics of running: how does stiffness couple with speed? *Journal of biomechanics*, 23:65–78, 1990.

[54] MENG X., WANG S., CAO Z., and ZHANG L. A review of quadruped robots and environment perception.

[55] Middleditch A. and Oliver J. *Functional anatomy of the spine*. Elsevier Health Sciences, 2005.

[56] Narita Y.and Kuratani S. Evolution of the vertebral formulae in mammals: a perspective on developmental constraints. *Journal of Experimental Zoology Part B: Molecular and Developmental Evolution*, 304(2):91–106, 2005.

[57] Papadopoulos E. and Koutsoukis K. On passive quadrupedal bounding with flexible linear torso. *International Journal of Robotics, Theory and Applications*, 4(2):1–8, 2016.

[58] Pouya S., Khodabakhsh M., Spröwitz A., and Ijspeert A. Spinal joint compliance and actuation in a simulated bounding quadruped robot. *Autonomous Robots*, pages 1–16, 2015.

[59] Pusey J.L. and Yoo J.H. Validation and verification of a high-fidelity computational model for a bounding robot's parallel actuated elastic spine. In *SPIE Defense+ Security*, pages 90840G–90840G. International Society for Optics and Photonics, 2014.

[60] Rosendo A., Nakatsu S., Narioka K., and Hosoda K. Pneupard: A biomimetic musculoskeletal approach for a feline-inspired quadruped robot. In *2013 IEEE/RSJ International Conference on Intelligent Robots and Systems*, pages 1452–1457. IEEE, 2013.

Publications based on this Thesis

1. Bhattacharya, Shounak, and Ashitava Ghosal. "*Design of a one-dimensional flexible structure for desired load-bearing capability and axial displacement*", Mechanics Based Design of Structures and Machines,(Under review) 2017.

2. Bhattacharya, Shounak, and Ashitava Ghosal. "Flexible spine modeling for quadruped robot.", Dynamic Walking 2017, Åland Island,Finland.